

Special Section:The Arctic: An AGU Joint
Special Collection**Key Points:**

- The atmosphere-ecosystem carbon exchange of a heterogeneous boreal landscape was determined
- Peatlands (26% area) contributed 22% total carbon dioxide (CO₂) uptake and 89% methane (CH₄) emission; forests offset 6% CH₄ emission and water bodies 7% CO₂ uptake
- Differentiating between noninundated drier and inundated wetter peatlands improved radiative effect estimates

Supporting Information:

Supporting Information may be found in the online version of this article.











Correspondence to:D. Kou,
dan.kou@uef.fi;
dan.kou1120@gmail.com**Citation:**Kou, D., Virtanen, T., Treat, C. C., Tuovinen, J.-P., Räsänen, A., Juutinen, S., et al. (2022). Peatland heterogeneity impacts on regional carbon flux and its radiative effect within a boreal landscape. *Journal of Geophysical Research: Biogeosciences*, 127, e2021JG006774. <https://doi.org/10.1029/2021JG006774>

Received 22 DEC 2021

Accepted 7 SEP 2022

Author Contributions:**Conceptualization:** Dan Kou, Tarmo Virtanen, Claire C. Treat, Juha-Pekka Tuovinen, Alekski Räsänen, Qianlai Zhuang, Atte Korhola, Narasinha J. Shurpali**Data curation:** Dan Kou, Tarmo Virtanen, Claire C. Treat, Juha-Pekka Tuovinen, Alekski Räsänen, Sari Juutinen,

Peatland Heterogeneity Impacts on Regional Carbon Flux and Its Radiative Effect Within a Boreal Landscape

Dan Kou^{1,2} , Tarmo Virtanen³, Claire C. Treat⁴ , Juha-Pekka Tuovinen⁵ , Alekski Räsänen^{3,6} , Sari Juutinen³, Juha Mikola^{3,7} , Mika Aurela⁵, Lauri Heiskanen⁵ , Maija Heikkilä³, Jan Weckström³, Teemu Juselius³, Sanna R. Piilo³, Jia Deng⁸ , Yu Zhang⁹, Nitin Chaudhary^{10,11}, Conghong Huang¹² , Minna Väiliranta³, Christina Biasi¹ , Xiangyu Liu² , Mingyang Guo² , Qianlai Zhuang² , Atte Korhola³, and Narasinha J. Shurpali¹³

¹Biogeochemistry Research Group, Department of Biological and Environmental Sciences, University of Eastern Finland, Kuopio, Finland, ²Department of Earth, Atmospheric, and Planetary Sciences, Purdue University, West Lafayette, IN, USA, ³Ecosystems and Environment Research Programme, Faculty of Biological and Environmental Sciences, and Helsinki Institute of Sustainability Science (HELSUS), University of Helsinki, Helsinki, Finland, ⁴Permafrost Research Section, Alfred Wegener Institute Helmholtz Centre for Polar and Marine Research, Potsdam, Germany, ⁵Finnish Meteorological Institute, Helsinki, Finland, ⁶Natural Resources Institute Finland (Luke), Oulu, Finland, ⁷Carbon Cycle Management, Department of Bioeconomy and Environment, Natural Resources Institute Finland, Helsinki, Finland, ⁸Earth Systems Research Centre, Institute for the Study of Earth, Oceans and Space, University of New Hampshire, Durham, NH, USA, ⁹Canada Centre for Remote Sensing, Natural Resources Canada, Ottawa, ON, Canada, ¹⁰Department of Geosciences, University of Oslo, Oslo, Norway, ¹¹Department of Physical Geography and Ecosystem Science, Lund University, Lund, Sweden, ¹²Department of Epidemiology and Environmental Health, University at Buffalo, Buffalo, NY, USA, ¹³Production Systems, Natural Resources Institute Finland, Maaninka, Finland

Abstract Peatlands, with high spatial variability in ecotypes and microforms, constitute a significant part of the boreal landscape and play an important role in the global carbon (C) cycle. However, the effects of this peatland heterogeneity within the boreal landscape are rarely quantified. Here, we use field-based measurements, high-resolution land cover classification, and biogeochemical and atmospheric models to estimate the atmosphere-ecosystem C fluxes and the corresponding radiative effect (RE) for a boreal landscape (Kaamanen) in northern Finland. Our result shows that the Kaamanen catchment currently functioned as a sink of carbon dioxide (CO₂) and a source of methane (CH₄). Peatlands (26% of the area) contributed 22% of the total CO₂ uptake and 89% of CH₄ emissions; forests (61%) accounted for 78% of CO₂ uptake and offset 6% of CH₄ emissions; water bodies (13%) offset 7% of CO₂ uptake and contributed 11% of CH₄ emissions. The heterogeneity of peatlands accounted for 11%, 88%, and 75% of the area-weighted variability (deviation from the area-weighted mean among different land cover types (LCTs) within the catchment) in CO₂ flux, CH₄ flux, and the combined RE of CO₂ and CH₄ exchanges over the 25-year time horizon, respectively. Aggregating peatland LCTs or misclassifying them as nonpeatland LCTs can significantly ($p < 0.05$) bias the regional CH₄ exchange and RE estimates, while differentiating between drier noninundated and wetter inundated peatlands can effectively reduce the bias. Current land cover products lack such details in peatland heterogeneity, which would be needed to better constrain boreal C budgets and global C-climate feedbacks.

Plain Language Summary Peatlands form part of the boreal landscapes exhibiting diverse types and microforms that have different characteristics of topography, hydrology, vegetation, and soil. Our understanding is still limited concerning how boreal peatlands, especially their inherent heterogeneities, affect the regional biosphere-atmosphere exchange of carbon and related climate effects, and what level of detail is needed to characterize them in land cover maps. By combining remote sensing information, field measurements, and biogeochemical modeling, we showed that, among different land cover types, peatlands played a dominant role in the variability of methane (CH₄) flux (88%) and the combined radiative climate effect due to carbon dioxide and CH₄ exchanges (75% over the 25-year time horizon). Possible aggregation and misclassification of peatland types could induce significant biases in the regional CH₄ balances and radiative effect estimates, but the distinction of noninundated drier and inundated wetter peatland types could reduce these biases effectively.

© 2022. The Authors.

This is an open access article under the terms of the [Creative Commons Attribution License](https://creativecommons.org/licenses/by/4.0/), which permits use, distribution and reproduction in any medium, provided the original work is properly cited.

Juha Mikola, Mika Aurela, Lauri Heiskanen

Formal analysis: Dan Kou, Tarmo Virtanen, Claire C. Treat, Juha-Pekka Tuovinen, Alekski Räsänen

Funding acquisition: Christina Biasi, Atte Korhola, Narasinha J. Shurpali

Investigation: Dan Kou, Tarmo Virtanen, Claire C. Treat, Juha-Pekka Tuovinen, Alekski Räsänen, Sari Juutinen, Juha Mikola, Mika Aurela, Lauri Heiskanen, Maija Heikkilä, Jan Weckström, Teemu Juselius, Sanna R. Piilo, Minna Väiliranta

Methodology: Dan Kou, Tarmo Virtanen, Claire C. Treat, Juha-Pekka Tuovinen, Alekski Räsänen, Jia Deng, Yu Zhang, Xiangyu Liu, Mingyang Guo, Qianlai Zhuang

Visualization: Dan Kou, Tarmo Virtanen, Claire C. Treat, Juha-Pekka Tuovinen, Alekski Räsänen

Writing – original draft: Dan Kou, Tarmo Virtanen, Claire C. Treat, Juha-Pekka Tuovinen, Alekski Räsänen, Atte Korhola, Narasinha J. Shurpali

Writing – review & editing: Dan Kou, Tarmo Virtanen, Claire C. Treat, Juha-Pekka Tuovinen, Alekski Räsänen, Sari Juutinen, Juha Mikola, Mika Aurela, Lauri Heiskanen, Maija Heikkilä, Jan Weckström, Teemu Juselius, Sanna R. Piilo, Jia Deng, Yu Zhang, Nitin Chaudhary, Conghong Huang, Minna Väiliranta, Christina Biasi, Mingyang Guo, Qianlai Zhuang, Atte Korhola, Narasinha J. Shurpali

1. Introduction

The boreal biome, consisting of forest (80%), peatland (15%), and lake (5%) ecosystems, occurs in continental interiors south of the treeless tundra at 45–71°N and covers about 15 million km² or 10% of Earth's land surface area (Helbig et al., 2020; Olson et al., 2001). It is characterized by a cool climate with relatively low precipitation and the dominance of coniferous forests. This vast and patterned area stores more carbon (C) than the atmosphere (~1,000 vs. 860 GtC), a large part of which resides under the ground, especially in peatland (Bradshaw & Warkentin, 2015; Friedlingstein et al., 2020; Gorham, 1991; Hugelius et al., 2020). Moreover, the boreal ecosystems are vulnerable to environmental changes (Åberg et al., 2010; Hoppole et al., 2020; Loisel et al., 2021), and thus, their functioning in the changing climate is vital to the global C budget (Comyn-Platt et al., 2018; Gauthier et al., 2015; Tagesson et al., 2020).

Landscape processes are important for the upscaling of C budget across a biome since Earth System Models (ESMs) or statistical C flux assessments are generally performed based on grid cells that are composed of multiple land units (Lawrence et al., 2018; Virkkala et al., 2021). A typical boreal landscape shows a mosaic of diverse forests, peatlands, and water bodies with large differences in their abiotic and biotic characteristics (Chapin et al., 2011; Hugelius et al., 2020; Verpoorter et al., 2014). During the past decades, our understanding of the landscape-scale C dynamics, including both carbon dioxide (CO₂) and methane (CH₄), in the circumpolar region is mainly derived from tundra (Sturtevant & Oechel, 2013; Treat et al., 2018; Weller et al., 1995) and the transition zone between the tundra and boreal biomes (Christensen et al., 2007; O'Shea et al., 2014; Tang et al., 2015). Within the boreal biome, most studies have been aimed at the C dynamics of individual ecosystems (Clemmensen et al., 2013; Guo et al., 2020; Johansson et al., 2006) or the entire boreal zone (Kicklighter et al., 2019; Tagesson et al., 2020) with only a few landscape-scale studies that include both CO₂ and CH₄ exchanges with the atmosphere and consider forest, peatland, and aquatic ecosystems at the same time. These studies have advanced our understanding, for example, by showing the difference between short- and long-term C dynamics within a catchment (Juutinen et al., 2013), the need for integrating terrestrial and aquatic fluxes at the landscape scale (Aurela et al., 2015; Chi et al., 2020; Juutinen et al., 2013), and the application of airborne measurements of CO₂ and CH₄ fluxes to regional upscaling (O'Shea et al., 2014).

Boreal peatlands show high spatial variability in ecotypes and microforms due to varying topography and hydrological conditions leading to different vegetation and soil characteristics. However, our understanding is still limited concerning how this heterogeneity affects regional biosphere-atmosphere C fluxes and related radiative effects (RE) of a boreal landscape, and what level of detail is needed to characterize the boreal peatlands to better constrain regional C budgets. Recently, there have been multiple attempts to produce local, regional, national, and circumpolar databases of northern peatlands. In part of these attempts, all peatlands and wetlands have been lumped into one class (Hird et al., 2017; Hugelius et al., 2020; Karlson et al., 2019; Tanneberger et al., 2017; Xu et al., 2018), but there exist approaches that separate peatland types, such as different bogs and fens (Amani et al., 2017; Bourgeau-Chavez et al., 2017; Korpela et al., 2020; Mahdianpari et al., 2020; Olefeldt et al., 2021; Räsänen & Virtanen, 2019). Currently, the most detailed circumpolar database (BAWLD) uses existing GIS data sets and machine learning modeling to estimate the fractional coverage of five different wetland classes in 0.5° grid cells (Olefeldt et al., 2021). Also some other data products have relied on existing GIS databases (Hugelius et al., 2020; Tanneberger et al., 2017; Xu et al., 2018), while others have used remotely sensed data that enable construction of higher spatial resolution data sets (Amani et al., 2017; Bourgeau-Chavez et al., 2017; Hird et al., 2017; Karlson et al., 2019; Mahdianpari et al., 2020; Räsänen & Virtanen, 2019). In view of the diverse attempts in delineating peatlands, it is urgent for us to have a better understanding of the regional effects of the peatland-dominated heterogeneity so that we can determine the level of detail to characterize heterogeneous boreal peatlands. This is important to improve remote sensing-based upscaling products and procedures, current C inventories, and especially ESMs, in which the peatlands are considered as a single block entity, if at all (Loisel et al., 2021).

To fill this knowledge gap, we conducted an in-depth study in a boreal catchment located in northern Finland. We asked how the peatlands and their heterogeneity affect regional biosphere-atmosphere C budgets and related RE by considering all land cover types (LCTs) within the catchment, and what level of detail is needed to characterize the heterogeneous peatlands. To answer these questions, we first produced a high-resolution land cover classification based on multisource remote sensing and field data. Second, by utilizing terrestrial and aquatic biogeochemical models and field observations, we quantified the daily and annual C dynamics (i.e., CO₂, CH₄,

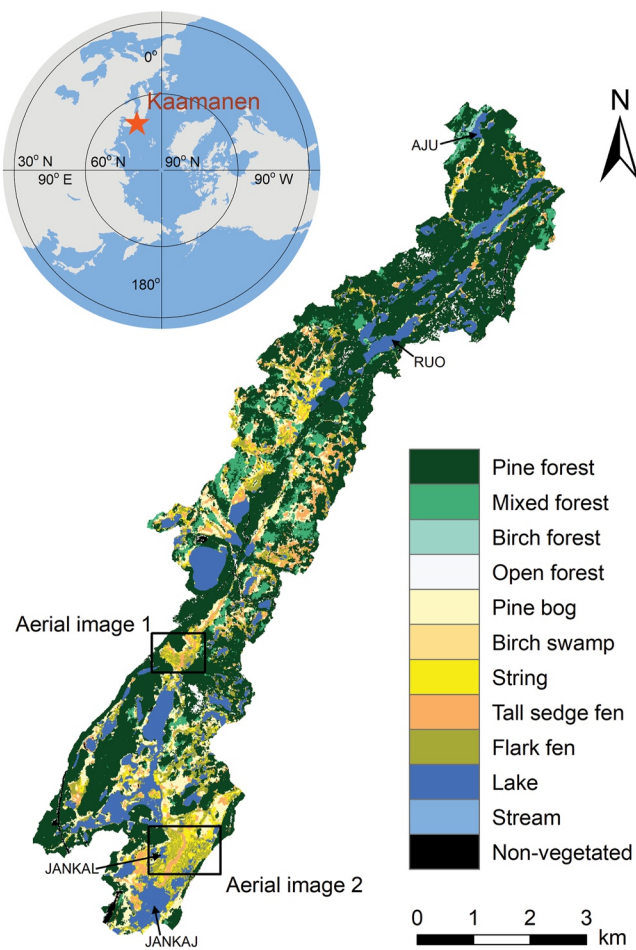


Figure 1. Location and land cover types of the Kaamanen catchment. The areas labeled as Aerial images 1 and 2 correspond to panels (a) and (b) in Figure 2, respectively. AJU (Annan Juomusjärvi), RUO (Ruohojärvi), JANKAL (Jänkälampi), and JANKAJ (Jänkäjärvi) are the four lakes with measurements in the catchment.

and total C budget) of each LCT and across the landscape and analyzed the role of peatlands in the landscape-scale C budget and the variability of C dynamics among LCTs. Moreover, we elucidated the role of peatlands in the RE variability of C exchanges among LCTs. Third, we evaluated how LCT aggregation or potential misclassification affected the estimation of regional C budgets and their RE. To assess the need for improved peatland mapping within the boreal zone, we further surveyed how accurately the peatland heterogeneity within the study area is depicted in current global, continental, and national land cover products and how these classifications affect the regional C budget and its RE modeled for the Kaamanen catchment.

2. Materials and Methods

2.1. Study Area

This study was conducted in a 32.8 km² boreal catchment situated in northern Finland (69.13–69.26°N, 27.21–27.45°E; 155 m a.s.l.), about 200 km south of the Arctic Ocean (Figures 1 and 2). We delineated the catchment using a 10-m resolution digital terrain model and the VALUE tool (<http://paikkitieto.ymparisto.fi/value/>). The catchment is characterized by a subarctic climate (Aurela et al., 2001). The mean annual air temperature during the period from 1981 to 2010 at the Inari Ivalo weather station (59 km south of Kaamanen) was -0.4°C with the warmest and coldest monthly air temperature being 14.0°C and -12.8°C in July and January, respectively (Pirinen et al., 2012). During the aforementioned period, the mean annual precipitation was 472 mm, and the mean annual relative humidity was 79% (Pirinen et al., 2012). The catchment is located within the sporadic permafrost zone, but no permafrost has been found there anymore in recent decades (Fronzek et al., 2010).

2.2. Land Cover Classification

We classified the LCTs using a geographic object-based image analysis approach, following the methodology described by Räsänen et al. (2019) and Räsänen and Virtanen (2019). Object-based approaches have been documented to be effective in particular when analyzing high-spatial resolution remote sensing imagery (Blaschke et al., 2014; Chen et al., 2018), and it has

been shown that inclusion of multisource (i.e., multiple types of remote sensing data) and multi-temporal remote sensing data increases land cover classification accuracy (Amani et al., 2017; Chasmer et al., 2020; Halabisky et al., 2018; Karlson et al., 2019; Räsänen & Virtanen, 2019). Specifically, we segmented a WorldView-2 satellite image (WV-2, DigitalGlobe Inc, Westminster, CO, USA) using a full lambda schedule segmentation with an average segment size of 0.2 ha. For each segment, we calculated 352 features, including spectral, topographic, vegetation height, and texture features, from the WorldView-2 image, four PlanetScope satellite images (PS, Planet Labs Inc, San Francisco, CA, USA) in different phenological stages and aerial lidar data (National Land Survey of Finland) (Table S1 in Supporting Information S1).

We collected training data from 16 transects of 0.25–1.0 km in length and visual interpretation of an aerial orthophoto. In total, there were 1,058 training segments (18–383 in each LCT). We used a supervised random forest classification (Breiman, 2001) to classify the segments into 11 LCTs (excluding streams) (Table 1; Figures 1 and 2, Figure S1 in Supporting Information S1). We assessed the accuracy of the classification with a pixel-based approach utilizing 359 vegetation plots, of which 137 were circular plots with a radius of 5 m (of which 59 were in transects and 78 randomly sampled), 204 were quadrats with a 50 cm side length (in transects), and 18 were circular plots with a radius of 20 cm (Räsänen & Virtanen, 2019).

After the random forest classification, we added the stream LCT to the map from National Land Survey of Finland topographic database. We split the fen string LCT into string top and string margin fractions considering

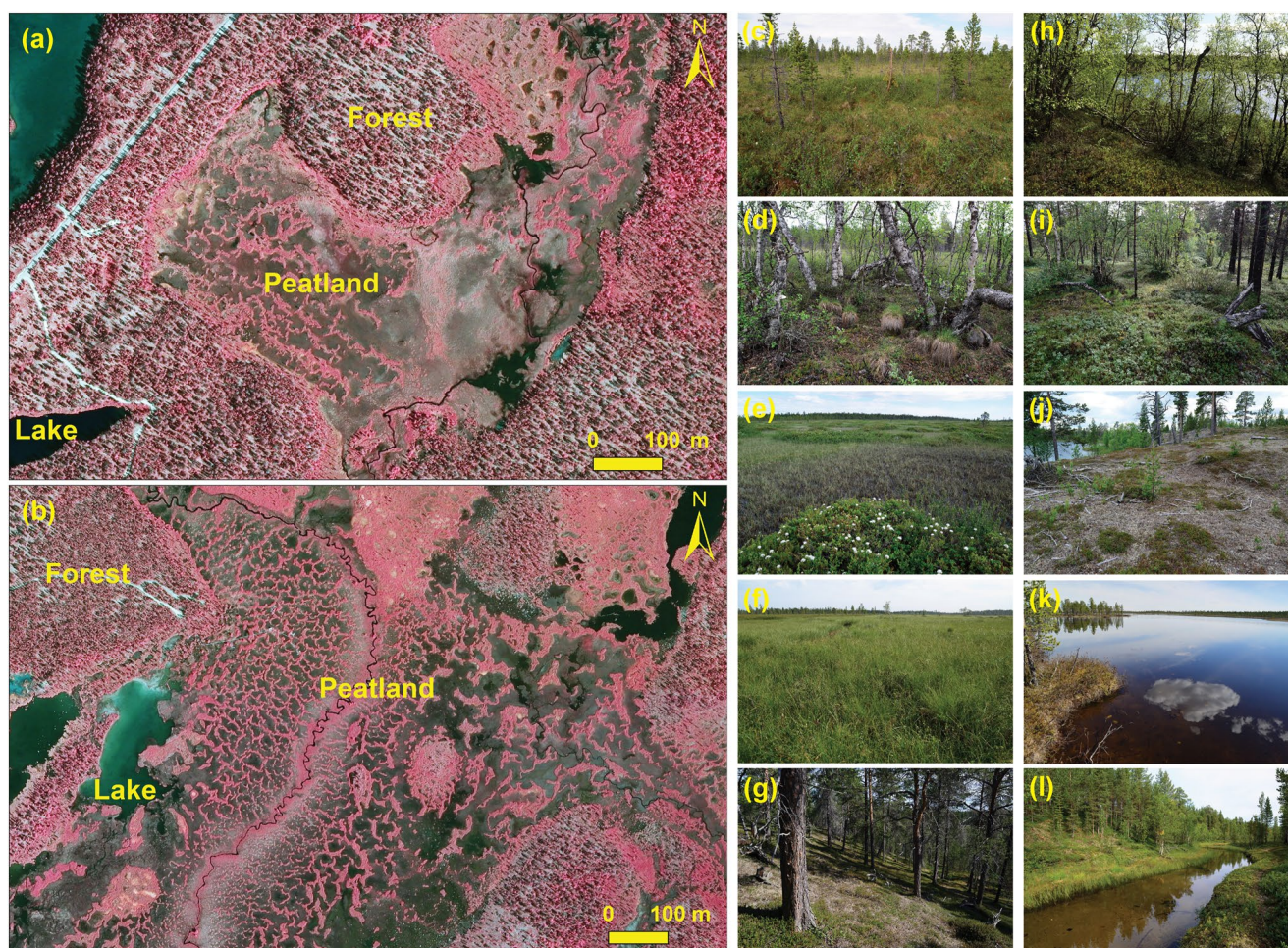


Figure 2. 0.5-m resolution false color aerial images (a) and (b) and photographs of different land cover types (c–l) of the Kaamanen catchment. (a) and (b) correspond to the Aerial image 1 and 2 areas, respectively in Figure 1. (c–l) represent pine bog, birch swamp, string (hummock in panel e) and flark fen (hollow in panel e), tall sedge fen, pine forest, birch forest, mixed forest, open forest, lake, and stream, respectively. For peatlands, pine bog, birch swamp, and string are relatively drier peatland types, and flark fen and tall sedge fen are relatively wetter types.

their large differences in hydrology and C dynamics (Figures S2–S7 and Table S2 in Supporting Information S1). We assumed that 59.2% of the string belong to tops and 40.8% to margins based on the results of 5-cm resolution land cover classification conducted for a peatland area within the study landscape (Heiskanen et al., 2021; Räsänen & Virtanen, 2019) (Table 1).

2.3. Flux Measurements

Measurements of the CO₂ and CH₄ fluxes of the dominant peatland LCTs, that is, pine bog, string top, string margin, tall sedge fen, and flark fen, were from Juutinen et al. (2013) and Heiskanen et al. (2021). Chamber flux measurements were made during three intensive campaigns from July to September and once in June in 2005, biweekly from early June to late September and once in October in 2006 (Juutinen et al., 2013), six times between 12 June and 11 October 2017, and seven times between 31 May and 4 September 2018 (Heiskanen et al., 2021) (Figures S2–S13 and Table S3 in Supporting Information S1). Permanent chamber bases were installed in spatial replicate for the above-mentioned peatland types, and the chamber size was 56 × 56 cm × height 30 cm in 2005 and 2006, 60 × 60 cm × height 30 cm in 2017, and 60 × 60 cm × height 40 cm in 2018 (Heiskanen et al., 2021; Juutinen et al., 2013). The chamber collar volume was taken into account when calculating the flux. Net ecosystem CO₂ exchange (NEE) was measured using transparent chambers equipped with a fan and an infrared gas analyzer (in 2005–2006, EGM-3, PP-systems, MA, USA; in 2017–2018, Picarro G2401, Picarro Inc, CA, USA) and was determined from several (2–4) replicate measurements. Ecosystem respiration (ER) was measured

Table 1
Land Cover Types, Their Areal Fraction, and Dominant Species in the Tree, Understory, and Ground Layers

Land cover type	Areal fraction (%)	Tree layer	Field layer	Ground layer
Pine forest	52.89	Canopy cover >10%, pine (<i>Pinus sylvestris</i>) cover >2/3 of total canopy cover	Evergreen shrubs (e.g., <i>Vaccinium vitis-idaea</i> , <i>Empetrum nigrum</i> , and <i>Calluna vulgaris</i>) and also some deciduous shrubs	Feather mosses and lichens
Birch forest	0.43	Canopy cover >10%, birch (<i>Betula pubescens</i>) cover >2/3 of total canopy cover	Evergreen and deciduous shrubs	Feather mosses and lichens
Mixed forest	5.91	Multiple tree species, including pine, birch, and few aspen (<i>Populus tremula</i>), canopy cover >10%, cover of minority species >1/3	Evergreen (<i>Vaccinium vitis-idaea</i>) and deciduous (<i>Vaccinium myrtillus</i> and <i>Vaccinium uliginosum</i>) shrubs	Feather mosses and lichens
Open forest	1.34	Forest with tree canopy cover <10%	Evergreen shrubs and some deciduous shrubs	Lichens, and some feather mosses
Pine bog	9.32	Peatland with coverage of pine trees >1%	Evergreen (<i>Rhododendron tomentosum</i>) and deciduous (<i>Vaccinium uliginosum</i> , <i>Betula nana</i>) shrubs, and some forbs (<i>Rubus chamaemorus</i>) and graminoids (mostly <i>Carex</i> spp.)	<i>Sphagnum</i> , feather mosses, and lichens
Birch swamp	0.12	Peatland with coverage of birch trees >2%	Forbs, grasses, and shrubs	<i>Sphagnum</i> and feather mosses
String top	2.65	Peatland with few trees (<1% coverage)	Evergreen and deciduous dwarf shrubs as well as forbs (esp. <i>Rubus chamaemorus</i>)	<i>Sphagnum</i> and feather mosses, and some lichens
String margin	1.83	Peatland with few trees (<1% coverage)	<i>Betula nana</i> , other dwarf shrubs, and some sedges	<i>Sphagnum</i> , dry and wet mosses
Tall sedge fen	5.64	None	Sedges, also deciduous shrubs (e.g., <i>Betula nana</i> , <i>Salix</i> spp.), and forbs	<i>Sphagnum</i> , wet brown mosses, and open water
Flark fen	5.97	None	Grasses and forbs	Open water, bare peat, and wet brown mosses
Lake	13.16	None	None	Open water
Stream	0.06	None	None	Open water
Nonvegetated	0.67	None	None	Mostly human made bare areas, sand with some stones, and all roads in the area

using opaque chambers. The chamber closure duration for detection of CO₂ flux was about 2–3 min (Heiskanen et al., 2021; Juutinen et al., 2013). Fluxes were calculated from the mean mixing ratio change in time using linear regression based on ordinary least squares (Heiskanen et al., 2021; Juutinen et al., 2013). Gross primary productivity (GPP) was calculated as the difference between NEE and ER. In 2005–2006, CH₄ fluxes were measured using opaque chambers equipped with a fan. The chamber closure duration for detection of CH₄ flux was over 20 min in Juutinen et al. (2013) and 2 min in Heiskanen et al. (2021). CH₄ concentration in the samples of chamber air was determined using gas chromatographs (HP-5710A and HP-5890A, Palo Alto, CA, USA) (Juutinen et al., 2013). In 2017–2018, CH₄ and CO₂ fluxes were measured at the same time with a portable gas analyzer (Heiskanen et al., 2021). Chamber measurements for terrestrial fluxes were generally conducted between 09:00 and 16:00 local standard time (Heiskanen et al., 2021).

In the pine forest (69.1°N, 27.3°E), NEE was measured using the eddy covariance (EC) technique from June 2017 to December 2018 (Heiskanen et al., 2022). The forest around the flux tower was about 50 years old due to logging, but most of the pine forests within the catchment are pine-dominated older-growth forests with an uneven age distribution. The NEE data for birch forest were derived from the EC measurements conducted at Petsikko (69.28°N, 27.14°E) in June–September 1996 (Aurela, Tuovinen, & Laurila, 2001). Flux data were lacking for the mixed forest and open forest LCTs. Fluxes of CO₂ and CH₄ were measured in four lakes (i.e., Jänkälampi, Annan Juomusjärvi, Ruohojärvi, and Jänkäjärvi) within the catchment during June–October 2017 (Figure 1). The two lakes in the northern catchment, that is, Annan Juomusjärvi and Ruohojärvi, were deeper,

maximum depths up to 9 m, while the lakes in the southern part, that is, Jänkälampi and Jänkjärvi, were shallow with a maximum depth of 1–1.5 m. All but lake Jänkjärvi had sandy bottoms and mineral rich sediments. Sediment of Lake Jänkjärvi had high organic content. Gas fluxes were measured using floating closed chambers. In Lake Jänkälampi, we used a chamber having area of 60×60 cm and height of 30 cm (Heiskanen et al., 2022). Concentrations of CO_2 and CH_4 inside the chamber were analyzed with a Picarro G2401 (Picarro Inc, CA, USA). In all, fluxes were measured during five campaigns. These measurements were conducted at 20 m from the north shore of the lake with 3–25 individual measurements per measurement day including both daytime and nighttime. For each measurement, the chamber closure time was 7 min, after which the chamber was ventilated for 3 min to get the inside concentration back to ambient. On 10 June 2017, 16 flux measurements in total were conducted at five spots on a 20-m-long transect from the shore toward the center of the lake. Each of the nine measurements from the first four spots were within the mean \pm standard deviation of the seven measurements made at the 20-m reference spot, indicating that there was no obvious spatial variation of flux along the transect. All lake measurements were conducted with floating chambers that were opened and closed with a pulley system from the shore so that the lake sediments were not disturbed. The other much larger lakes (Annan Juomusjärvi, Ruohojärvi, and Jänkjärvi) were measured biweekly during June–August 2017. During each measurement occasion, a set of five chambers (volume of 8 L and an area of 0.05 m^2) were distributed along the lake's radius to capture the spatial variation in water depth and in distance to the shoreline. During the 30–60 min closure, four samples of chamber air were drawn using a 60-ml polyethene syringe. The samples were stored in 12 ml glass vials flushed with sample air prior their analysis using a gas chromatograph equipped with EC, TC, and FI detectors (Agilent 7890B, with Gilson GX271 autosampler). Samples were analyzed within a month from the sampling (Heiskanen et al., 2022). Positive fluxes in this study indicate a C flux to the atmosphere, while negative values represent C uptake by the ecosystem.

2.4. Terrestrial Ecosystem Modeling

Ecosystem C dynamics of the terrestrial land cover types in the study landscape were simulated using a process-based biogeochemistry model, NEST-DNDC (Treat et al., 2018; Zhang et al., 2012). It integrates a biogeochemical model DeNitrification-DeComposition (DNDC) (Kou et al., 2020; Li et al., 2000) with the Northern Ecosystem Soil Temperature model (NEST) (Zhang et al., 2003). In the model, all LCTs share common climate and atmospheric environmental conditions (e.g., atmospheric CO_2 and nitrogen (N) concentrations), but they differ in their assigned land types, soil, hydrology, and vegetation characteristics.

In this study, the simulations with the NEST-DNDC model for the terrestrial LCTs were conducted through the following three steps. First, we prepared the data sets required for model input, including daily climate, soil profiles, hydrological parameters, and vegetation conditions. The climate data set included daily mean, maximum, and minimum air temperatures, precipitation, wind speed, global radiation, and relative humidity from 2005 to 2018. They were derived from observations at the Inari Kaamanen weather station (69.14°N , 27.27°E) located within the Kaamanen catchment with missing data filled with observations at the Inari Väylä (69.07°N , 27.49°E) and Inari Ivalo (68.61°N , 27.42°E) weather stations. In addition, we used climate data from the Utsjoki Kevo weather station (69.76°N , 27.01°E) in 1996 to calibrate the model for the birch forest at Petsikko.

The LCT-specific soil variables mainly included texture, pH, and soil C concentration (Table S2 in Supporting Information S1). The soil texture was loamy sand for forests determined based on a previous study near Kaamanen (Köster et al., 2014) and organic soil for peatlands. In all peatlands, we collected soil samples of a known volume from layers 0–5 cm and 15–20 cm beneath the litter layer (the layer where vascular plant and moss leaf structures are still discernible) using a knife and scissors. We dried the samples (48 hr at 75°C) and weighted for dry mass. Parts of the dry samples were ground using a ball mill and 0.2 g subsamples of ground material were analyzed for soil C concentrations using a LECO CNS-2000 analyzer (LECO Corporation, Saint Joseph, MI, USA). Soil pH was estimated in the field in water collected at the depth of 30 cm. In pine, birch, and pine-birch mixed forests, we dug pits to a depth of 100 cm and collected horizontal soil cores (length 5 cm, diameter 3 cm) from the organic (O) and eluvial (E) horizons, from the top and bottom parts of the illuvial (B) horizon, and at the depth of 50 and 100 cm. We then analyzed soil C concentration and pH for these samples. The hydrology data mainly included water table, which were derived from Juutinen et al. (2013) and Heiskanen et al. (2021) (Table S2 in Supporting Information S1). Vegetation data included in the models consisted of aboveground plant biomass and leaf area index (LAI) of different LCTs (Tables S4 and S5 in Supporting Information S1). We determined the aboveground

biomass and LAI of each LCT based on 130 circular plots with a radius of 5 m (71 random plots, 59 plots in transects) distributed among the LCTs (see Text S1 in Supporting Information S1 for more detailed information).

Second, we calibrated and validated the model for different LCTs (Figures S2–S15 in Supporting Information S1). The observed C fluxes used for the model calibration included the 1,996 data of birch forest, the 2006 data of pine bog, string margin, tall sedge fen, and flark fen, and the 2017 data of string top and pine forest. The calibrated models were then validated with the remaining C flux data, from 2005 for pine bog, string margin, tall sedge fen, and flark fen, from 2017 for string margin, and from 2018 for string top, string margin, and pine forest. Finally, we ran the calibrated and validated model to simulate daily C dynamics of the dominant terrestrial LCTs and used the daily fluxes to calculate the annual C budgets for the period 2005–2018. The C budget of mixed forest and open forest was simulated based on parameters from pine/birch forest and their own soil and vegetation data. The pine bog simulation was also used for birch swamp (covering only 0.12% of study area) in the landscape-scale estimation of C budget and RE since observations were lacking for birch swamp.

2.5. Aquatic Ecosystem Modeling

The Arctic Lake Biogeochemistry Model (ALBM), which is a one-dimensional process-based climate-sensitive lake biogeochemistry model (Guo et al., 2020; Tan et al., 2015, 2017), was used to simulate the lake CO₂ and CH₄ fluxes in the study area. For lake C fluxes, the model simulates both the diffusive and ebullitive emissions. The model was first calibrated against observations of water temperature and C fluxes of the lake using the Monte Carlo method with 10,000 parameter sample sets. The optimum parameter set was then selected based on the total root-mean-square error of the modeled CO₂ and CH₄ fluxes. Finally, we performed simulations over the same period forced by the same meteorological data as for the other LCTs (Figure S16 in Supporting Information S1). The model calibration, parameter optimization, and simulation were performed for each of the four lakes with measurements in the catchment (i.e., Jänkälampi, Annan Juomusjärvi, Ruohojärvi, and Jänkäjärvi) (Figure 1 and Figure S16 in Supporting Information S1). The mean simulated fluxes of these four lakes were used in the study to reflect the average level of the catchment lake fluxes. The lake simulations were also used for streams in the landscape-scale estimation of C budget and RE.

2.6. Radiative Effect of Greenhouse Gas Fluxes

The annual CO₂ and CH₄ fluxes (g m⁻² yr⁻¹) of each LCT during the period of 2005–2018 were used as input to estimate the radiative effect of these fluxes, that is, their contribution to Earth's radiative balance. We expressed this effect as the cumulative RE due to an annual emission or uptake pulse over time horizons of 25 and 100 years, which was calculated using a dynamic radiative forcing (RF) model (Lohila et al., 2010; Mathijssen et al., 2017; Piilo et al., 2020). These time horizons are shorter and longer, respectively, than the time taken to reach the steady state determined by the CH₄ emission and atmospheric oxidation rates (Myhre et al., 2013). Even though we used a RF model here, it is important to note that we refer to this quantity as RE, as the present-day greenhouse gas (GHG) fluxes, in contrast to long-term C accumulation in peatland or a change in these fluxes, do not induce a forcing that would result from a perturbation to Earth's energy balance (Neubauer, 2021; Taillardat et al., 2020). This modeling is performed in order to obtain a common metric for the CO₂ and CH₄ fluxes in a similar vein to the CO₂-equivalent fluxes derived from the global warming potential concept; however, using RE as the common metric provides additional flexibility as we can dynamically account for the effect of changing background concentrations.

In the RF model, CO₂ and CH₄ pulses were assumed to be instantaneously and completely mixed in the atmosphere (Myhre et al., 2013). The resulting atmospheric concentration pulses were modeled to decay according to characteristic time scales related to global biogeochemical cycles. For CO₂, these dynamics were implemented as a weighted sum of four exponential functions, where the shortest perturbation time was 4.3 years and the slowest decay function effectively corresponded to a permanent atmospheric change for 22% of the pulse (Joos et al., 2013). The evolution of the atmospheric CH₄ concentration perturbation was calculated as an exponential decay with a single atmospheric perturbation time scale of 12.4 years (Myhre et al., 2013).

Atmospheric oxidation of the emitted CH₄ molecules to CO₂, which generates an indirect RE, was included in the model assuming an 80% efficiency for the CH₄-to-CO₂ conversion (Boucher et al., 2009). The instantaneous RE resulting from the modeled CO₂ and CH₄ concentration changes was calculated with a radiative efficiency parameterization (Etminan et al., 2016). This parameterization takes into account the spectral interactions between CO₂,

CH₄, and nitrous oxide. The model also includes an estimate for the indirect CH₄-induced RE due to ozone and stratospheric water vapor changes (Myhre et al., 2013). The RE due to ecosystem-atmosphere fluxes was calculated as a marginal change with respect to specified, variable background concentrations (Lohila et al., 2010). In this study, these concentrations were adopted from the Representative Concentration Pathway (RCP) 4.5 scenario (Meinshausen et al., 2011) and the total RE refers to the sum of the RE due to CO₂ and CH₄.

2.7. Heterogeneity and Uncertainty Analysis

The landscape-scale C budget and RE were estimated by weighting the C budget and RE of each LCT (except nonvegetated) with the corresponding relative area within the catchment. The role of the landscape-scale heterogeneity of peatlands in C budget and RE was quantified at two levels based on the LCT-specific C fluxes expressed (a) per unit area (“LCT-based heterogeneity”) and (b) as area-weighted budgets (“area-based heterogeneity”). For the LCT-based heterogeneity, we calculated the sum of squared deviations (SSD) from the arithmetic mean among peatland LCTs and that among all LCTs within the landscape and then divided the peatland SSD by the landscape SSD. For the area-based heterogeneity, we calculated the ratio between the SSD from the area-weighted mean among peatland LCTs and that among all LCTs within the boreal landscape. In the LCT-based heterogeneity, all dominant LCTs in the catchment were considered, including pine bog, string top, string margin, tall sedge fen, flark fen, pine forest, birch forest, mixed forest, and open forest. In the area-based heterogeneity, all LCTs except nonvegetated area were considered.

To elucidate the uncertainty in the landscape-scale results due to aggregation or misclassification of peatlands, we tested the statistical difference among different land cover classification cases, in which the original peatland LCTs were combined or peatlands were misclassified as nonpeatland LCTs with a least significant difference (LSD). Combining peatland LCTs is relevant because peatland LCTs in the current circumpolar peatland maps are generally expressed as a uniform land cover type (Hugelius et al., 2020; Xu et al., 2018) without capturing the spatial heterogeneity among different peatland types. In remote sensing-based products, peatlands can also be confused with other terrestrial or aquatic LCTs. Most commonly, forested peatland is misclassified as forest (Thompson et al., 2016) and open water-logged peatland with sparse vegetation as a lake (Matthews et al., 2020).

We considered four LCT aggregation cases: (a) all peatland LCTs were identified as noninundated drier peatland with the mean flux of drier peatland LCTs (APDP); (b) all peatland LCTs were identified as inundated wetter peatlands with the mean flux of wetter peatland LCTs (APWP); (c) all peatland LCTs were identified as generic peatlands with the mean flux of all peatland LCTs (APGP); (d) all wetter peatland LCTs were identified as generic wetter peatlands and all drier peatland LCTs were identified as generic drier peatlands with the corresponding mean fluxes (WWDD). In addition, we designed three cases in which the peatland LCTs were misclassified: (a) all peatland LCTs were replaced by other terrestrial and aquatic LCTs (no peatland); (b) forested peatlands (pine bog and birch swamp) were incorrectly identified as the corresponding forests (pine and birch forest, respectively) (FPF); (c) open wetter peatlands with sparse vegetation (flark fen) were incorrectly identified as lakes (OWPSVL).

2.8. Survey of Land Cover Products

We surveyed different land cover products available for our study area, including seven global maps complemented by one continental and one national map (Table 2). We assessed how well peatlands are presented in them by calculating the fractional peatland/wetland area and estimating the spatial agreement with our LCT data by error matrices (Frey & Smith, 2007; Krankina et al., 2008).

In addition, we assessed how the differences in these land cover products affect the regional C and RE budgets estimated for the Kaamanen catchment. To estimate the regional C budgets, we matched the LCTs of each product to our LCT classification. Specifically, for GLCC, *Evergreen Needleleaf Forest* = *pine forest* and *Closed Shrublands* = *average of pine bog and string top*; for MODIS.LCT, *Evergreen Needleleaf Forests* = *pine forest* and *Woody Savannas/Savannas* = *average of pine bog and string top*; for GLC2000, *Tree Cover (needle-leaved, evergreen)/Mosaic (Tree cover/Other natural vegetation)* = *pine forest*, *Shrub Cover (closed-open, deciduous (with or without sparse tree layer))* = *average of pine bog and string top*, and *Regularly flooded shrub and/or herbaceous cover* = *average of tall sedge fen and flark fen*; for GlobCover2009, *Open (15%–40%) needleleaved deciduous or evergreen forest (>5m)*/*Mosaic forest or shrubland (50%–70%) (grassland (20%–50%))* = *pine forest*, *Mosaic grassland (50%–70%) (forest or shrubland (20%–50%))*/*Sparse (<15%) vegetation* = *average of pine bog and string top*, *Closed to open (>15%) grassland or woody vegetation on regularly flooded or waterlogged soil - Fresh, brackish or saline water* = *average*

Table 2
Assessment of Peatland/Wetland Representation in Different Land Cover Products for the Kaamanen Boreal Landscape

Product	Reference	Scale	Version	Methodology	Spatial resolution	Peatland/wetland relevant class label	Peatland/wetland area (%)	Spatial agreement (%)
Global Land Cover Characterization (GLCC)	Loveland et al. (2000)	Global	Version 2	Remote sensing	1 km	–	0	0
Moderate Resolution Imaging Spectroradiometer Land Cover Type (MODIS.LCT)	Sulla-Menashe et al. (2019)	Global	MCD12Q1 v006	Remote sensing	500 m	–	0	0
Global Land Cover 2000 (GLC2000)	Bartholomé and Belward (2005)	Global	Global Product v1.1	Remote sensing	1 km	<i>Regularly flooded shrub and/or herbaceous cover</i>	58.0	21.8
Global Land Cover Map for 2009 (GlobCover2009)	Arino et al. (2012)	Global	v2.3	Remote sensing	300 m	<i>Closed to open (>15%) grassland or woody vegetation on regularly flooded or waterlogged soil</i>	0.1	0.1
First 10-m resolution global land cover product (FROM-GLC10)	Gong et al. (2019)	Global	v01	Remote sensing	10 m	<i>Wetland</i>	0.1	0.01
Global Lakes and Wetlands Database (GLWD)	Lehner and Döll (2004)	Global	Level 3	Database	30 s	–	0	0
PEATMAP	Xu et al. (2018)	Global	Finland	Meta-analysis	Shapefile	<i>Peatland</i>	24.8	48.5
CORINE Land Cover 2018 EU, 25 ha (CLC2018EU.25ha)	https://land.copernicus.eu/pan-european/corine-land-cover/clc2018	Continental	2018, 25 ha	Remote sensing and database	Shapefile (minimum unit 25 ha)	<i>Peatbog</i>	25.3	44.8
CORINE Land Cover 2018 FI, 20 m (CLC2018FI.20m)	https://ckan.ymparisto.fi/data%20set/corine-maanpeite-2018	National	2018, 20 m	Remote sensing and database	20 m	BFPL, CFPL, MFPL, TWPL, <i>peatbog</i> , TIM, and AIM	28.6	62.0

Note. BFPL, CFPL, MFPL, TWPL, TIM, and AIM indicate *Broad-leaved forest on peatland*, *Coniferous forest on peatland*, *Mixed forest on peatland*, *Transitional woodland/shrub cc 10%–30% on peatland (cc = canopy closure)*, *Terrestrial inland marsh*, and *Aquatic inland marsh*, respectively. The italic texts mean the peatland / wetland class names in land cover products.

of tall sedge fen and flark fen, and Water bodies = lake; for FROM-GLC10, forest = pine forest, grassland/shrubland/tundra = average of pine bog and string top, wetland = average of tall sedge fen and flark fen, water = lake, and Impervious surface/bareland/snow/ice = non-vegetated area; for CLC2018EU.25ha, Coniferous forest = pine forest, Peatbog = average of pine bog and string top, and Water body = lake; for CLC2018FI.20m, Broad-leaved forest on mineral soil = birch forest, Broad-leaved forest on peatland = birch swamp, Coniferous forest on mineral soil/Transitional woodland or shrub on mineral soil = pine forest, Mixed forest on mineral soil = mixed forest, Coniferous forest on peatland/Mixed forest on peatland/Transitional woodland or shrub on peatland = pine bog, Terrestrial inland marsh/Aquatic inland marsh = average of tall sedge fen and flark fen, Peatbog = average of pine bog and string top, Water course = stream, Water body = lake, and Artificial surface/Beach, dune, and sand plain = nonvegetated area.

3. Results

3.1. Landscape Heterogeneity

Thirteen LCTs were distinguished within the Kaamanen catchment using high spatial resolution land cover classification (Figure 1, Figure S1 in Supporting Information S1 and Table 1) with an overall accuracy of 73.1%

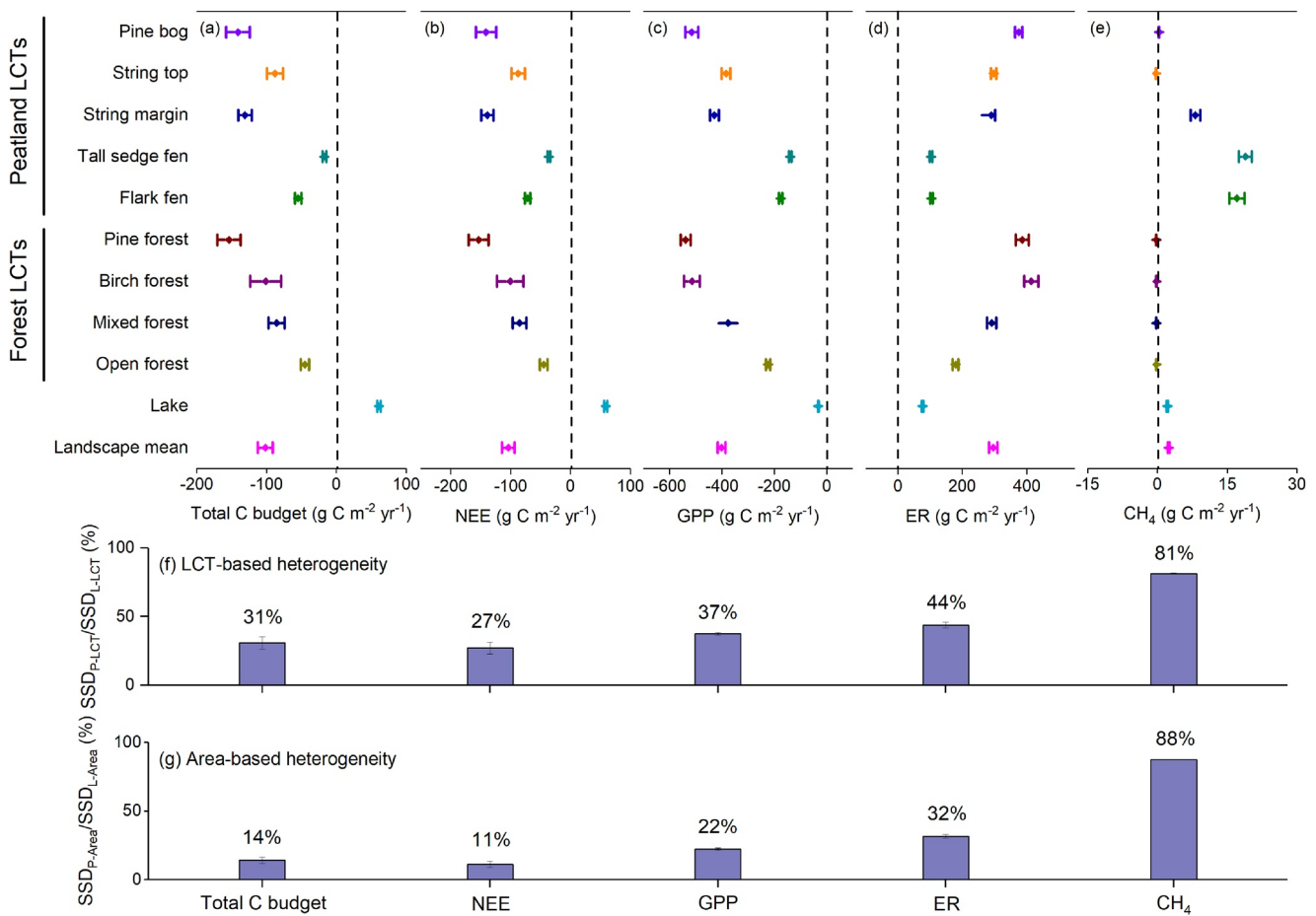


Figure 3. Heterogeneity in carbon (c) budget within the Kaamanen boreal landscape during 2005–2018. (a) Total C budgets combining carbon dioxide (CO₂) and methane (CH₄) among land cover types (LCTs) and their area-weighted landscape mean; (b) CO₂ budgets (net ecosystem CO₂ exchange); (c) gross primary productivity; (d) ecosystem respiration (ER); (e) CH₄ budgets; (f) ratio between the sum of squared deviations (SSD) from the arithmetic mean C budget among peatland LCTs (SSD_{P-LCT}) and that among all landscape LCTs (SSD_{L-LCT}); (g) ratio between the SSD from the area-weighted landscape mean among peatland LCTs (SSD_{P-Area}) and that among all landscape LCTs (SSD_{L-Area}). In panels (a–e), a positive value indicates C flux from the ecosystem to the atmosphere. The diamond symbol in panels (a–e) and the bar and number in panels (f–g) indicate the mean annual value, and the error bar in all panels denotes the 95% confidence interval. For peatlands, pine bog, birch swamp, and string are relatively drier peatland types, and flark fen and tall sedge fen are relatively wetter types.

(Table S6 in Supporting Information S1). Four of these LCTs were forests (i.e., pine, birch, mixed, and open forests, occupying 60.6% of the landscape), two were water bodies (i.e., lake and stream, 13.2%), one represents nonvegetated areas (0.7%), and six were peatlands (25.5%) that were distributed along a gradient from forests to water bodies (Table 1). Among the peatland LCTs, pine bog (9.3%), birch swamp (0.1%), and fen string (including thin, elongated, and smaller, rounded elevated microforms; 2.7% string top and 1.8% string margin) were characterized as drier communities as their water tables were below the peat surface (Table 1, Table S2 in Supporting Information S1). Of these, pine bog and birch swamp represent forested drier peatlands, while string top and margin represent open drier peatland habitats (Table 1). The two inundated peatland LCTs, that is, tall sedge fen (5.6%) and flark fen (6.0%), represent open wetter peatland habitats (Table 1 and Table S2 in Supporting Information S1).

3.2. Carbon Fluxes

The various LCTs differ in vegetation, soil, and hydrological characteristics (Figures S2–S16 in Supporting Information S1; Table 1; Tables S2, S4 and S5 in Supporting Information S1), leading to heterogeneity in the ecosystem-atmosphere fluxes of CO₂ and CH₄ (Figure 3). For the total C budget (sum of CO₂-C and CH₄-C budgets), the terrestrial LCTs (peatlands and forests) functioned as C sinks, while lakes functioned as a significant C

source during the period 2005–2018 (Figure 3a). Among the peatland LCTs, the C budget ranged from a large C sequestration in pine bog ($-141 \pm 17 \text{ g C m}^{-2} \text{ yr}^{-1}$) to a small sequestration in tall sedge fen ($-17 \pm 3 \text{ g C m}^{-2} \text{ yr}^{-1}$), while among the forest types, the largest C sink was found for pine forest ($-154 \pm 17 \text{ g C m}^{-2} \text{ yr}^{-1}$) and the smallest for open forest ($-45 \pm 6 \text{ g C m}^{-2} \text{ yr}^{-1}$) (Figure 3a). The variability and magnitude of the total C budget were dominated by CO_2 (Figure 3b). Most peatland LCTs emitted CH_4 to the atmosphere with the largest emission from the water-logged peatland LCTs (tall sedge fen: $19 \pm 1 \text{ g C m}^{-2} \text{ yr}^{-1}$; flark fen: $17 \pm 2 \text{ g C m}^{-2} \text{ yr}^{-1}$) (Figure 3e). Forests functioned as weak CH_4 sinks (-0.23 ± 0.02 to $-0.26 \pm 0.02 \text{ g C m}^{-2} \text{ yr}^{-1}$), while lakes were CH_4 sources ($2.13 \pm 0.14 \text{ g C m}^{-2} \text{ yr}^{-1}$) (Figure 3e).

Furthermore, we found that peatland LCTs accounted for $31 \pm 4\%$, $27 \pm 4\%$, $37 \pm 1\%$, and $44 \pm 2\%$ of the variability among all landscape LCTs in total C budget that combined CO_2 and CH_4 , NEE, GPP, and ER, respectively, and explained most of the variability ($81 \pm 0.5\%$) in CH_4 flux (Figure 3f). By weighting the CO_2 and CH_4 exchange rates of each LCT by the corresponding areas, the landscape-scale C budget was estimated to be $-102 \pm 11 \text{ g C m}^{-2} \text{ yr}^{-1}$ in 2005–2018 (landscape mean in Figure 3a). It was dominated by a mean CO_2 sink of $-104 \pm 11 \text{ g C m}^{-2} \text{ yr}^{-1}$, while the CH_4 emission was $2.39 \pm 0.19 \text{ g C m}^{-2} \text{ yr}^{-1}$ (landscape mean in Figures 3b and 3c). The peatlands (26% of the area) contributed 22% of the landscape total CO_2 uptake and 89% of the total CH_4 emissions. The forests (61%) accounted for 78% of the total CO_2 uptake and offset 6% of the total CH_4 emissions. Water bodies (13%) emitted both CO_2 and CH_4 , offsetting 7% of the landscape CO_2 uptake and comprising 11% of the landscape CH_4 emissions. Furthermore, we found that peatlands explained $14 \pm 2\%$, $11 \pm 2\%$, $22 \pm 1\%$, $32 \pm 1\%$, and $88 \pm 0.1\%$ of the area-weighted variability among all LCTs in the total C budget, CO_2 flux, GPP, ER, and CH_4 flux (Figure 3g).

3.3. Radiative Effect of Carbon Exchange

The different heterogeneities in CO_2 -C and CH_4 -C budgets, together with the different radiative impacts of CO_2 and CH_4 (Myhre et al., 2013), led to a further layer of LCT heterogeneity in the C flux effect on radiative balance (Figure 4). The total RE generated by CO_2 and CH_4 fluxes varied greatly among the peatland LCTs (Figure 4a). Specifically, pine bog had the greatest negative RE ($-37 \pm 4 \text{ fW m}^{-2}$ over the 100-year time horizon, $1 \text{ fW} = 10^{-15} \text{ W}$), followed by string top ($-25 \pm 3 \text{ fW m}^{-2}$). In contrast, tall sedge fen exhibited the largest positive RE among all the LCTs ($69 \pm 6 \text{ fW m}^{-2}$), followed by flark fen ($52 \pm 7 \text{ fW m}^{-2}$). Consequently, the RE generated by different peatland types spanned a range of 107 fW m^{-2} , which was about 1.6 times that among the forest and aquatic LCTs (68 fW m^{-2}) (Figure 4a).

The area-weighted total RE resulting from the CO_2 and CH_4 budgets was $-19 \pm 3 \text{ fW m}^{-2}$ per unit area of the region over the 100-year time horizon (CO_2 : $-29 \pm 3 \text{ fW m}^{-2}$; CH_4 : $10 \pm 1 \text{ fW m}^{-2}$) and $-2 \pm 1 \text{ fW m}^{-2}$ over the 25-year time horizon (CO_2 : $-11 \pm 1 \text{ fW m}^{-2}$; CH_4 : $8 \pm 1 \text{ fW m}^{-2}$) (landscape mean in Figures 4a–4c). Despite comprising 25.5% of the landscape area, we found that the variability among peatland types accounted for $73 \pm 3\%$ to $80 \pm 1\%$ of the variability in total RE at the LCT level and $57 \pm 4\%$ to $75 \pm 3\%$ when considering LCT areas, depending on the time horizon (Figures 4d and 4e).

3.4. Uncertainty Due To Biased Peatland Classification

Using the regional upscaling from the full LCT classification as a baseline, we analyzed the potential deviation in C budget and its RE for cases in which peatland LCTs were combined or misclassified as forests or lakes (Figure 5). We found that the aggregation or misclassification of peatlands types did not change the regional total C budget that combined CO_2 and CH_4 compared to the Baseline (Figure 5a). However, it can significantly alter the CH_4 budget and total RE (Figures 5b–5d, Figure S17 in Supporting Information S1).

When all the peatland LCTs in the catchment were identified as a single drier peatland LCT, we found that the magnitude of (negative) RE over the 100-year/25-year time horizons significantly increased (Figures 5b and 5c). In contrast, when all the peatland LCTs were lumped together as one wetter peatland, the magnitude of RE significantly decreased over the 100-year time horizon and changed to positive over the 25-year time horizon (Figures 5b and 5c). However, these biases could be significantly reduced if either the mean REs of all peatland LCTs were used for the upscaling or drier and wetter peatland LCTs were separated (Figures 5b and 5c). The latter option, that is, using different C fluxes for wetter and drier peatlands, resulted in the smallest biases in CH_4 budget and RE with respect to upscaling with the full LCT classification and flux variability (Figure 5). When all

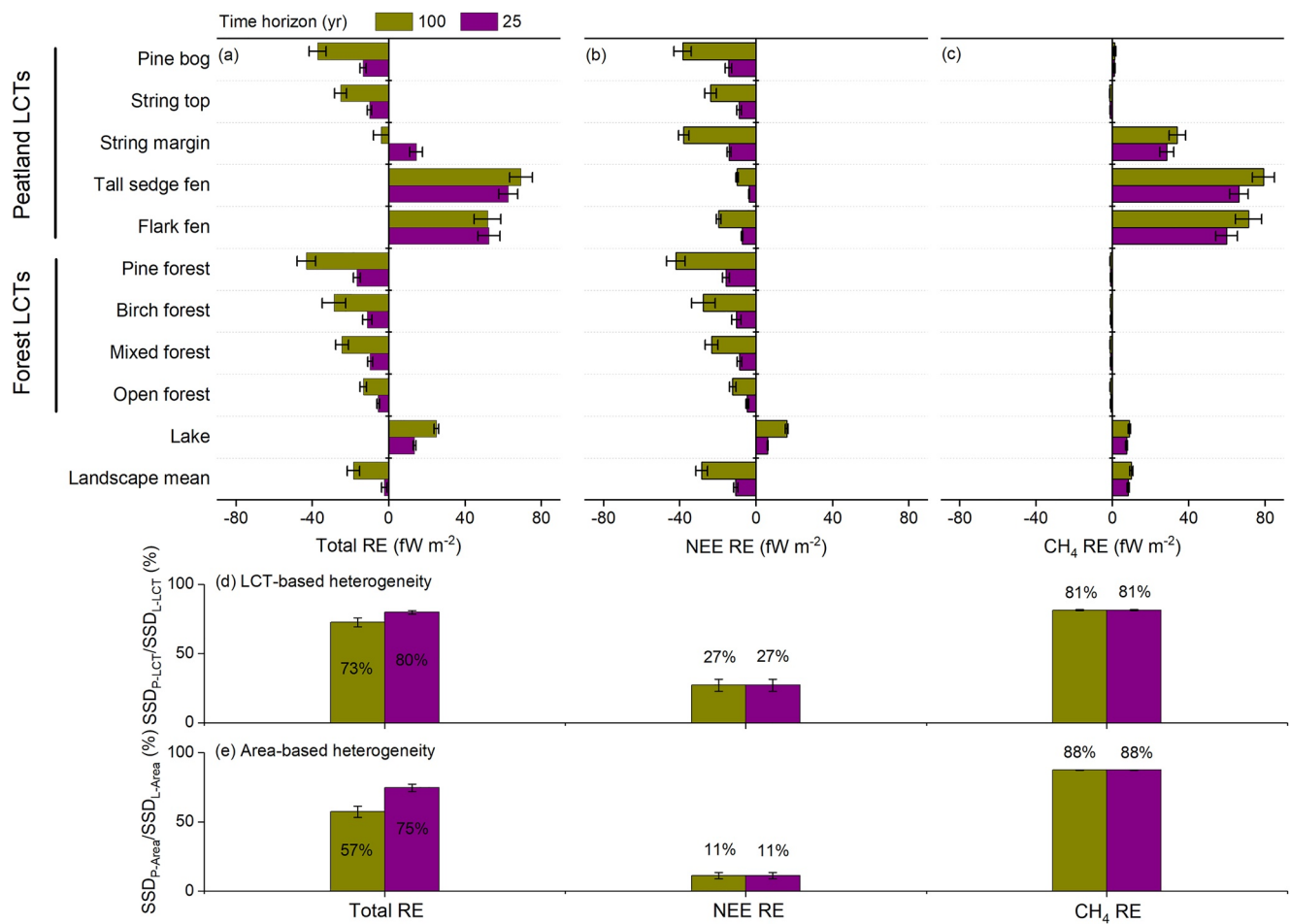


Figure 4. Heterogeneity in the radiative effect (RE) of present carbon (c) budget within the Kaamanen boreal landscape. (a) Total RE due to carbon dioxide (CO₂) and methane (CH₄) exchange of different land cover types (LCTs) and their area-weighted landscape mean; (b) RE due to CO₂ exchange (net ecosystem CO₂ exchange); (c) RE due to CH₄ exchange; (d) ratio between the Sum of Squared Deviations (SSD) from the arithmetic mean RE among peatland LCTs (SSD_{P-LCT}) and that among all landscape LCTs (SSD_{L-LCT}); (e) ratio between the SSD from the area-weighted landscape mean among peatland LCTs (SSD_{P-Area}) and that among all landscape LCTs (SSD_{L-Area}). The RE represents the cumulative RE due to an annual emission or uptake pulse over time horizons of 25 and 100 years, calculated based on C flux densities (g m⁻² yr⁻¹, i.e., flux per m² of each LCT) during 2005–2018 and assuming the RCP4.5 scenario. The diamond symbol in panels (a–c) and the bar and number in panels (d and e) indicate the mean annual value, and the error bar in all panels denotes the 95% confidence interval. 1fW = 10⁻¹⁵ W. For peatlands, pine bog, birch swamp, and string are relatively drier peatland types, and flark fen and tall sedge fen are relatively wetter types.

the peatland LCTs were replaced by other terrestrial and aquatic LCTs based on their areal fraction (the case of no peatland), the magnitude of RE significantly increased over both time horizons (Figures 5b and 5c). RE was also significantly altered over the 25-year time horizon when the open water-logged peatland with sparse vegetation cover (flark fen) was classified as lake (Figure 5c).

3.5. Survey of Different Land Cover Products

Compared to the 25.5% areal coverage of peatlands within the Kaamanen landscape revealed by our classification, there was no peatland/wetland specified in the global land cover map of GLCC, MODIS.LCT, or GLWD; the coverage was 0.1% in both GlobCover2009 and FROM-GLC10, as high as 58.0% in GLC2000, and 24.8% in PEATMAP (Figure 6; Table 2). Although the proportion of peatlands was similar in PEATMAP and this study, the spatial agreement between their areas was only 48.5% (Table 2). The corresponding spatial agreement for GLC2000, GlobCover2009, and FROM-GLC10 was 21.8%, 0.1%, and 0.01%, respectively (Table 2). Regarding the peatland/wetland heterogeneity, there was only one peatland/wetland type defined in any of the surveyed global products with different definitions, for example, “regularly flooded shrub and/or herbaceous cover” in GLC2000, “closed to open (>15%) grassland or woody vegetation on regularly flooded or waterlogged

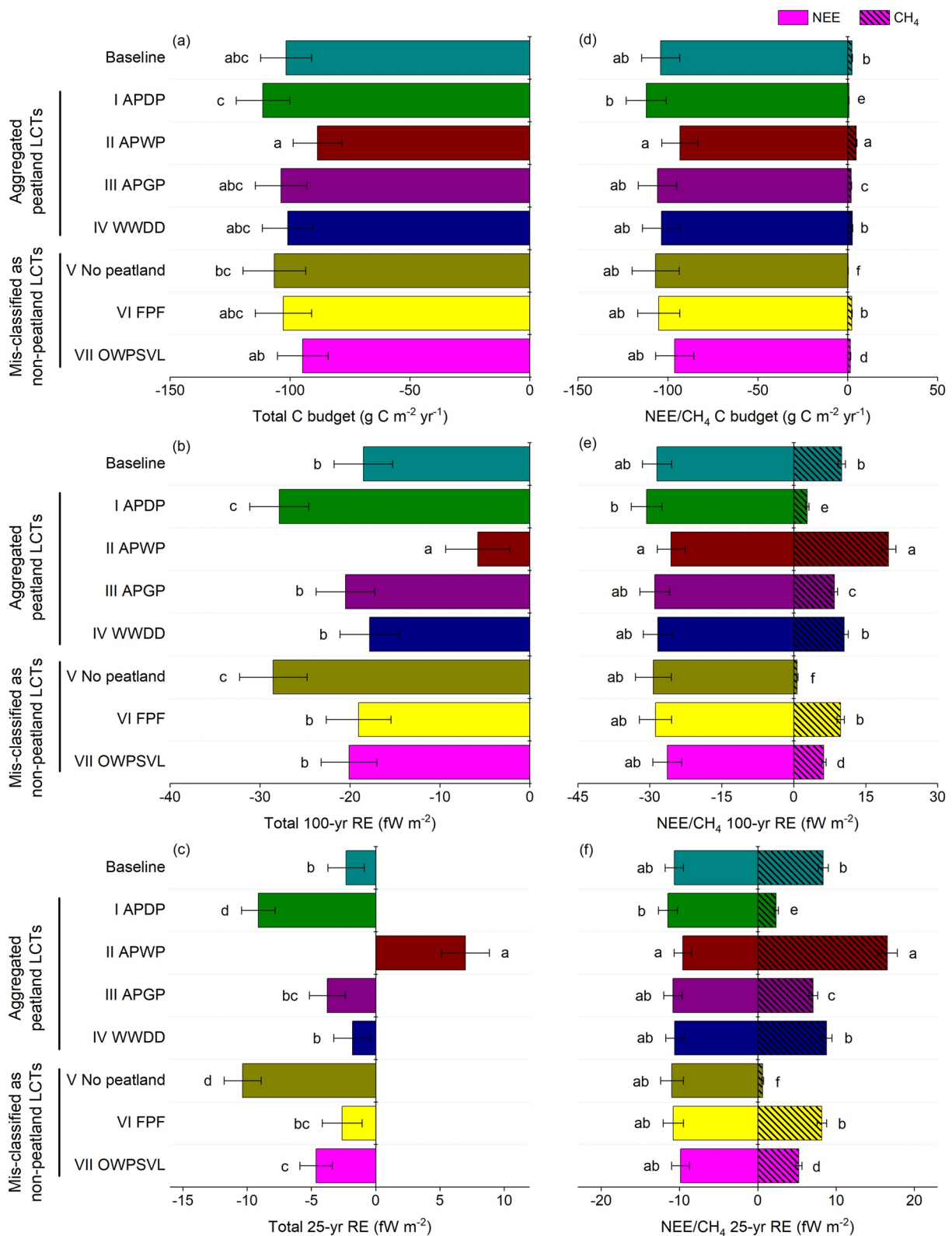


Figure 5.

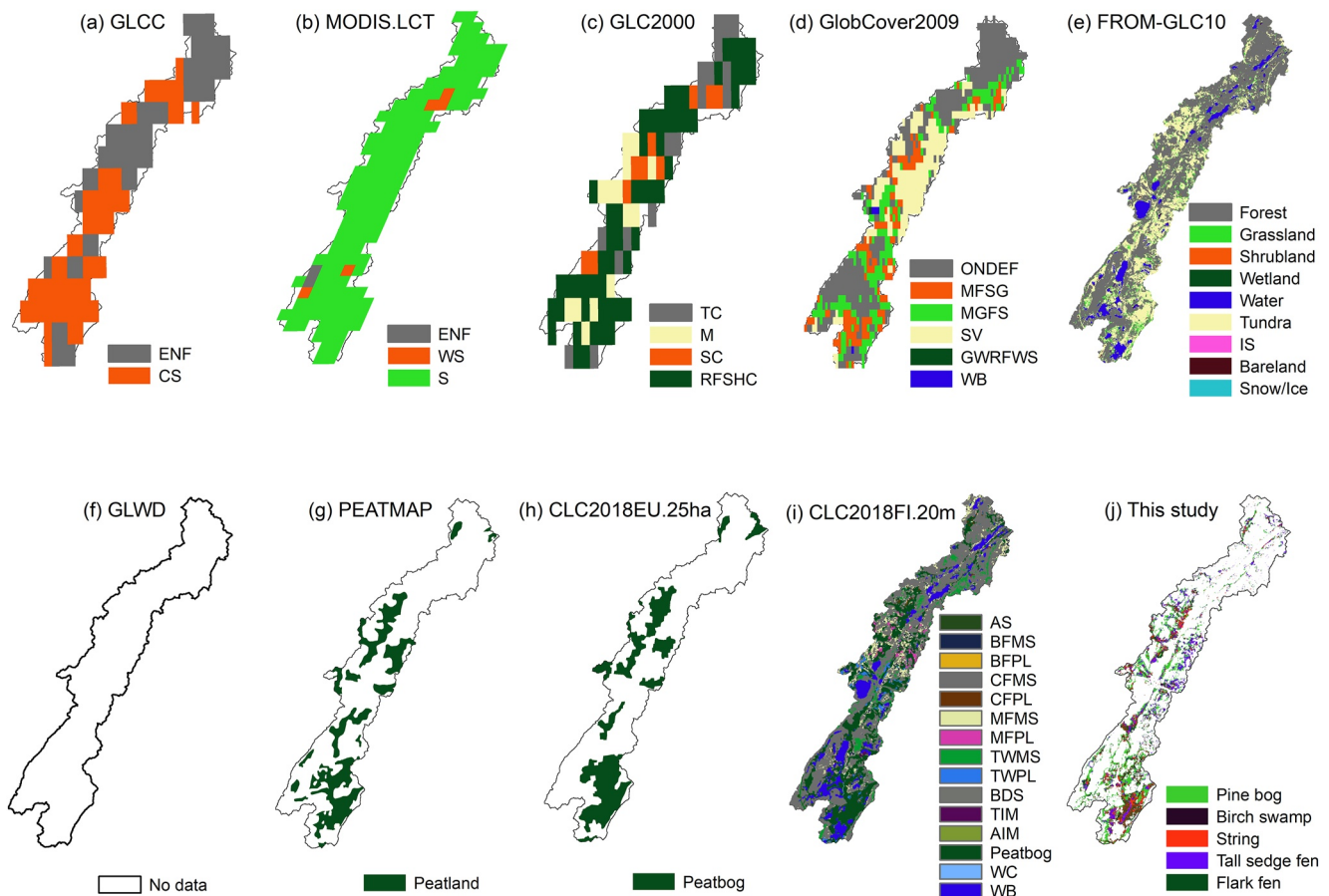


Figure 6. Land cover of the Kaamanen boreal landscape classified by global (a–g), continental (h), and national (i) land cover products and this study (j). (a) GLCC, (b) MODIS.LCT, (c) GLC2000, (d) GlobCover2009, (e) FROM-GLC10, (f) GLWD, (g) PEATMAP, (h) CLC2018EU.25ha, (i) CLC2018FI.20m, and (j) peatland types revealed by this study. For GLCC, ENF = *Evergreen Needleleaf Forest* and CS = *Closed Shrublands*, respectively; for MODIS.LCT, ENF = *Evergreen Needleleaf Forests*, WS = *Woody Savannas*, and S = *Savannas*, respectively; for GLC2000, TC = *Tree Cover (needle-leaved, evergreen)*, M = *Mosaic (Tree cover/ Other natural vegetation)*, SC = *Shrub Cover (closed-open, deciduous (with or without sparse tree layer))*, and RFSHC = *Regularly flooded shrub and/or herbaceous cover*, respectively; for GlobCover2009, ONDEF = *Open (15%–40%) needle-leaved deciduous or evergreen forest (>5m)*, MFSG = *Mosaic forest or shrubland (50%–70%)/grassland (20%–50%)*, MGFS = *Mosaic grassland (50%–70%)/forest or shrubland (20%–50%)*, SV = *Sparse (<15%) vegetation*, GWRFWFS = *Closed to open (>15%) grassland or woody vegetation on regularly flooded or waterlogged soil—Fresh, brackish or saline water*, and WB = *Water bodies*, respectively; for FROM-GLC10, IS = *Impervious surface*; for CLC2018EU.25ha, there are three classes within the Kaamanen landscape (*Coniferous forest, Peatbog, and Water body*) and only *Peatbog* is shown here; for CLC2018FI.20m, AS = *Artificial surface*, BFMS = *Broad-leaved forest on mineral soil*, BFPL = *Broad-leaved forest on peatland*, CFMS = *Coniferous forest on mineral soil*, CFPL = *Coniferous forest on peatland*, MFMS = *Mixed forest on mineral soil*, MFPL = *Mixed forest on peatland*, TWMS = *Transitional woodland/shrub on mineral soil*, TWPL = *Transitional woodland/shrub on peatland*, BDS = *Beach, dune, and sand plain*, TIM = *Terrestrial inland marsh*, AIM = *Aquatic inland marsh*, WC = *Water course*, and WB = *Water body*, respectively; for our classification, only peatland classes are shown here. More information about the land cover products is presented in Table 2.

Figure 5. Bias in landscape-scale carbon (C) budget and its radiative effect (RE) due to aggregation or misclassification of peatlands. (a) Landscape-scale total C budget combining carbon dioxide (CO₂) and methane (CH₄) during 2005–2018. (b and c) Total RE calculated based on landscape-scale total C budget over 100-year and 25-year time horizons; (d) Landscape-scale CO₂ (net ecosystem CO₂ exchange) and CH₄ budgets; (e and f) RE calculated based on landscape-scale CO₂ and CH₄ budgets over 100-year and 25-year time horizons. RE is calculated based on the C budget during 2005–2018 assuming the RCP4.5 scenario. Baseline is estimated based on the full land cover type (LCT) classification described in Table 1. I–IV are cases that peatland LCTs are aggregated and V–VII are cases that peatland LCTs are misclassified as nonpeatland LCTs. I, APDP, refers to All Peatland LCTs, was identified as noninundated Drier Peatland with the mean flux of drier peatland LCTs; II, APWP, refers to All Peatland LCTs, was identified as inundated Wetter Peatland with the mean flux of wetter peatland LCTs; III, APGP, refers to All Peatland LCTs, was identified as Generic Peatland with the mean flux of all peatland LCTs; IV, WWDD, refers to all Wetter peatland LCTs, was identified as generic Wetter peatland and all Drier peatland LCTs were identified as generic Drier peatland with corresponding mean fluxes; V, no peatland, refers to all peatland LCTs, was replaced by other terrestrial and aquatic LCTs based on their areal fraction; VI, FPF, refers to forested peatlands (pine bog and birch swamp), was identified as corresponding forests (pine and birch forest, respectively); VII, OWPSVL, refers to Open Wetter Peatlands with Sparse Vegetation (flark fen), was identified as Lake. For peatlands in this study, pine bog, birch swamp, and string are relatively drier peatland types, and flark fen and tall sedge fen are relatively wetter types. The bar and error bar in the plot represent the mean value and its 95% confidence interval, respectively, and the letters denote the statistical difference among different scenarios. The CH₄ budget in panel d is shown with a more limited scale in Figure S17 in Supporting Information S1. IfW = 10⁻¹⁵ W.

soil” in GlobCover2009, “wetland” in FROM-GLC10, and “peatland” in PEATMAP (Figure 6; Table 2). The European-level product, CLC2018EU.25ha, had a similar peatland representation to PEATMAP, that is, one peatland category (“*peatbog*”) with a 25.3% areal coverage and 44.8% spatial agreement (Figure 6; Table 2).

Compared to the global and continental scale products, the national database CLC2018FI.20m provided multiple peatland classes for the Kaamanen landscape (“*Broad-leaved forest on peatland*,” “*Coniferous forest on peatland*,” “*Mixed forest on peatland*,” “*Transitional woodland/shrub cc 10%–30% on peatland*” (cc = canopy closure), “*Peatbog*,” “*Terrestrial inland marsh*,” and “*Aquatic inland marsh*”) with the peatland area fraction and spatial agreement being 28.6% and 62.0%, respectively (Figure 6; Table 2). However, the “*Peatbog*” class defined as open peatlands smaller than 25 ha in CLC2018FI.20m (<https://ckan.ymparisto.fi/dataset/corine-maanpeite-2018>), alone occupied about 84% of the total peatland/wetland area (Figure 6i).

In addition, we found that the use of different land cover products resulted in significantly different estimates of the catchment-scale C and RE budgets (Figure 7). For the CO₂ budget and the total C budget combining CO₂ and CH₄ fluxes, the magnitude of the landscape-scale C sinks estimated with GLCC, GlobCover2009, FROM-GLC10, and CLC2018EU.25ha was significantly larger than those estimated with our detailed LCT mapping, while for GLC2000, they were significantly lower (Figures 7a and 7d). For the CH₄ budget, CLC2018FI.20m (0.17 g C m⁻² yr⁻¹) and FROM-GLC10 (0.03 g C m⁻² yr⁻¹) generated much smaller emissions than our mapping (2.4 g C m⁻² yr⁻¹), while GLC2000 overestimated substantially (10.4 g C m⁻² yr⁻¹); the others indicated minor CH₄ uptake (Figure 7d, Figure S18 in Supporting Information S1). Concerning both the 25-year and 100-year total RE, the large CH₄ emissions associated with GLC2000 generated a positive RE, while for the other land cover products, RE was negative but significantly larger in magnitude than for the LCT mapping of this study (Figures 7b and 7c).

4. Discussion

4.1. Landscape-Scale C Budgets in the Boreal Region

The results of this study improve our understanding of the level of detail needed to characterize the boreal peatlands to better constrain the landscape-scale C budget and its climate effect. This is motivated by the fact that peatlands are widespread across the boreal biome and boreal peatlands are generally heterogeneous (Heiskanen et al., 2021; Li et al., 2016). By overlapping the map of terrestrial ecoregions of the world (Olson et al., 2001) and the latest northern peatland map with 10-km pixels (Hugelius et al., 2020), we find that 94% of the pixels within the boreal biome contain peatlands (i.e., peatland area fraction >0) (Figure S19 in Supporting Information S1). Thus, distinguishing peatland areas and classes is highly relevant across the boreal region.

Our results showed that the area-weighted mean CO₂ sink across the open peatland area (including string, flark fen, and tall sedge fen) of the catchment during 2005–2018 was 69.6 g C m⁻² yr⁻¹, which is close to an open mire CO₂ sink of 69 g C m⁻² yr⁻¹ observed in a boreal landscape in northern Sweden in 2017 (Chi et al., 2020). The CH₄ emissions from our open peatland area, 14 g C m⁻² yr⁻¹, are also comparable to the emissions from this Swedish mire (10 g C m⁻² yr⁻¹) (Chi et al., 2020). Moreover, the CO₂ sink of our tall sedge fen (−36.3 g C m⁻² yr⁻¹) is close to the mean NEE of −38 g C m⁻² yr⁻¹ reported for wetlands in a synthesis of the data collected across the boreal biome (Virkkala et al., 2021), and the CH₄ emission of this LCT (19 ± 1 g C m⁻² yr⁻¹) is within the range (0–20 g C m⁻² yr⁻¹) of the majority of freshwater wetlands in the global FLUXNET-CH₄ Version 1.0 data set (Delwiche et al., 2021). The CO₂ sink among our forests ranged from 45 g C m⁻² yr⁻¹ in open forests to 153 g C m⁻² yr⁻¹ in pine forests, producing an area-weighted mean CO₂ sink of 144 g C m⁻² yr⁻¹, which is close to the CO₂ sink (150 g C m⁻² yr⁻¹ in 2017 and 173 g C m⁻² yr⁻¹ in 2018) observed in a 100-year-old forest in Sweden (Chi et al., 2020) and falls within the range reported for northern forests (Chi et al., 2021; Kljun et al., 2006; Kolari et al., 2004; Lindroth et al., 2020). The simulated average lake CO₂ budget in our catchment was about 61 g C m⁻² yr⁻¹, which is in a range between an annual net CO₂ source of 35 g C m⁻² yr⁻¹ observed at a lake called Pallasjärvi in northern Finland (Aurela et al., 2015; Lohila et al., 2015) and an annual mean efflux of 77 g C m⁻² yr⁻¹ observed at a lake in southern Finland (Huotari et al., 2011). In addition, our simulated average lake CH₄ budget (2.13 g C m⁻² yr⁻¹) falls within the range of 0.024–13.7 g C m⁻² yr⁻¹ in a summary of methane dynamics in different boreal lake types (Juutinen et al., 2009).

While extensive measurement data were available to us to constrain the estimation of the catchment-scale C budget, these data were compromised by some limitations that warrant further examination. First, the

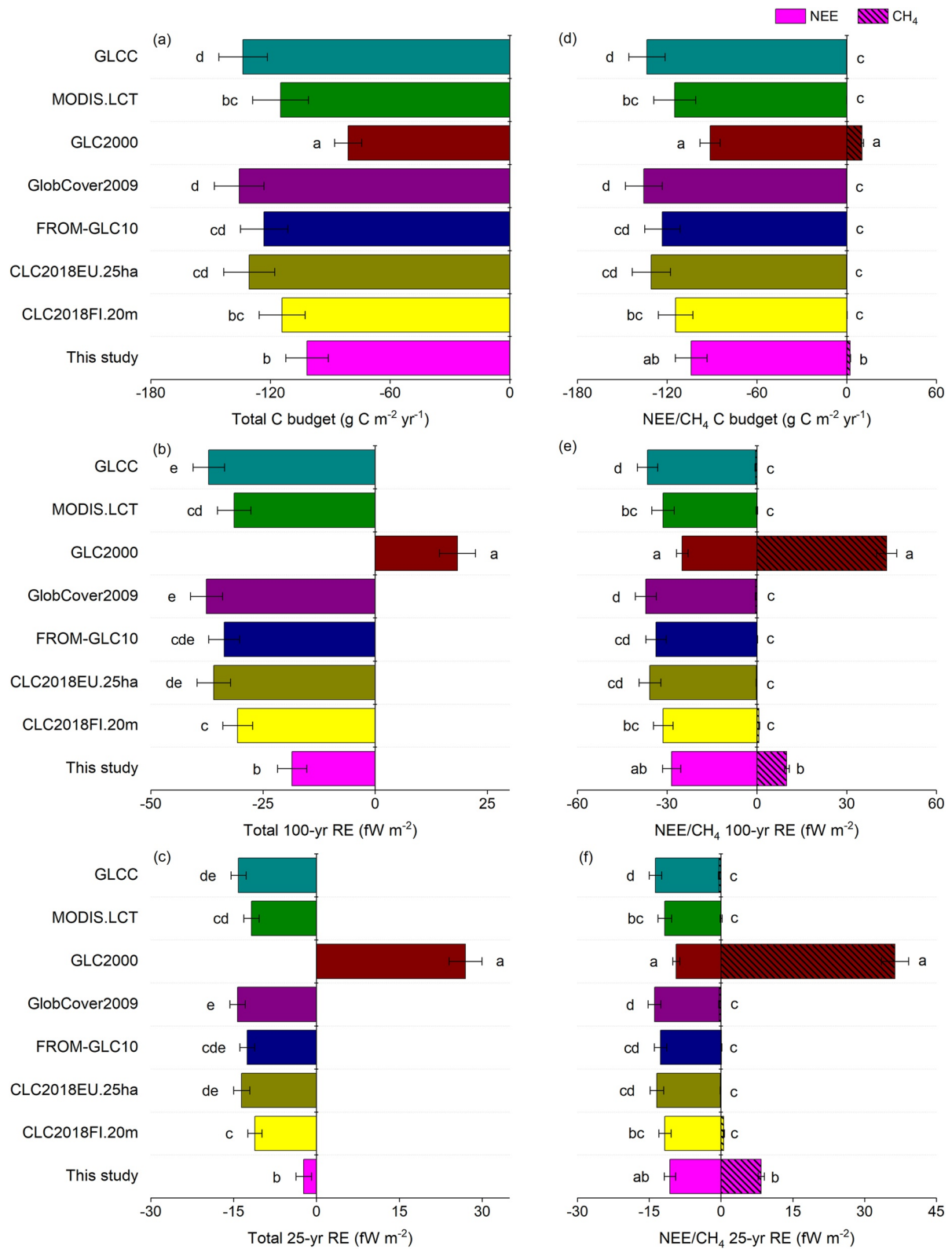


Figure 7.

stream-atmosphere C exchange was estimated from the lake data, which is likely to result in underestimated fluxes (Campeau et al., 2014; Dinsmore et al., 2010; Juutinen et al., 2013). In a study on the same catchment, Juutinen et al. (2013) found that the stream that traversed through the fen had high CO₂ and CH₄ effluxes with an average of 480 and 12 g C m⁻² yr⁻¹, respectively (the stream CO₂ and CH₄ effluxes used in this study were 61 and 2.1 g C m⁻² yr⁻¹, respectively). If using the data from Juutinen et al. (2013), the landscape-scale C budgets would be -104, 2.39, and -101 g C m⁻² yr⁻¹ for CO₂, CH₄, and total C flux, respectively, that is, practically the same as shown in Figure 3. Thus, using lake data for streams had no material effect here, which is obviously due to the small area of streams (0.06%). Second, only the diffusive CH₄ flux was used in the model calibration and validation of lake-atmosphere exchanges. Ebullition of CH₄ was measured in lakes and it was clearly largest in a shallow lake with organic sediments (Jänkjärvi). Heiskanen et al. (2022) quantified the ebullitive fluxes and found that ebullition formed 21% of the total CH₄ emissions from the entire lake area in that study.

Third, our chamber-based flux measurements used for model calibration and validation for most of the LCTs do not cover the nongrowing season, which cannot be regarded as negligible for the annual C budgets of northern ecosystems (Natali et al., 2019; Treat et al., 2018). The eddy covariance flux measurements for the pine forest used for this LCT show that our model captures some of the CO₂ efflux observed outside the growing season but it to some extent underestimates the nongrowing season total (simulated 17 g C m⁻², observed 37 g C m⁻² in January–April and November–December 2018) (Figure S14 in Supporting Information S1). Moreover, the previous EC data from the Kaamanen fen indicate that the wintertime CO₂ efflux from peatland area can be larger than the flux modeled here, while for the annual CH₄ emissions, this period is less important (Aurela et al., 2002; Heiskanen et al., 2021). Therefore, it is likely that we overestimated the magnitude of annual C sequestration of the Kaamanen catchment due to an insufficient modeling of the nongrowing season fluxes. The fourth limitation is that the age of the pine forest around the flux tower (50 years old due to logging) has some differences with the age of most of the pine forests within the catchment (pine-dominated older-growth forests with an uneven age distribution, and some more recently logged ones), which could generate some uncertainties in the pine forest's NEE of the studied catchment. Another potential limitation is the low temporal resolution of the chamber measurements, which could induce some unknown uncertainties to the annual C budget estimates.

4.2. Peatland Heterogeneity and Its Impact on Regional Carbon Budget and the Associated Radiative Effect

In this study, the peatland heterogeneity refers to the spatial variability of different peatland types and microforms. This variability results from topographical and hydrological variations leading to diverse vegetation and soil characteristics. Using high-resolution remote sensing images and field-based measurements, we classified the peatlands in the Kaamanen catchment into six types, including pine bog, birch swamp, string top, string margin, flark fen, and tall sedge fen. Pine bog and birch swamp represent treed peatlands, while the others are open peatlands. Among the open peatlands, tall sedge fen is found near water bodies (lakes/streams), while string and flark fen constitute the patterned open peatlands with hummock and hollow microforms. Based on the water table level, pine bog, birch swamp, and string can be characterized as relatively drier peatlands, while flark fen and tall sedge fen are relatively wetter.

Our results showed that the CO₂ sink among the diverse peatland classes ranged from 36 g C m⁻² yr⁻¹ in tall sedge fen to 141 g C m⁻² yr⁻¹ in pine bog. In addition, we found that peatlands explained 11% of the area-weighted CO₂ flux variability among all LCTs and that the aggregation or misclassification of peatland types did not change the regional CO₂ budget significantly compared to the Baseline derived from the accurate LCT classification (Figure 5). These results suggest that the identification of peatland heterogeneity may not have a particularly prominent impact on the regional CO₂ flux estimate.

For the CH₄ flux, however, the situation is different: we found that the peatlands in the Kaamanen catchment contributed 89% of the regional total CH₄ emissions and explained 88% of the area-weighted variability among

Figure 7. Landscape-scale carbon (C) budgets of the Kaamanen catchment and their radiative effects (RE) estimated based on different land cover products. (a) Total C budget combining carbon dioxide (CO₂) and methane (CH₄) during 2005–2018. (b and c) Total RE calculated from the total C budget over 100-year and 25-year time horizons; (d) CO₂ and CH₄ budgets; (e and f) RE calculated from the CO₂ and CH₄ budgets over 100-year and 25-year time horizons. RE is calculated from the C budget during 2005–2018 assuming the RCP4.5 scenario. The landscape-scale C budgets of this study were estimated based on the full land cover classification described in Table 1. The land cover types (LCTs) of other products were matched to our LCT classification so that we could estimate their C budgets and related RE. The vertical axis of the plot shows different land cover products (Table 2). The bar and error bar in the plot represent the mean value and its 95% confidence interval, respectively, and the letters denote the statistical difference among different products. The CH₄ budget in panel d is shown with a more limited scale in Figure S18 in Supporting Information S1. 1fW = 10⁻¹⁵ W.

all LCTs. While such a high degree of heterogeneity in CH₄ fluxes is previously known (Kuhn et al., 2021), our results clearly demonstrate how typical aggregation or misclassification of peatlands significantly alters the magnitude of the regional CH₄ flux estimate (Figure 5). Since CH₄ is a much stronger GHG than CO₂ (Myhre et al., 2013), such a classification error also significantly changed the magnitude, even the sign, of RE that combined CO₂ and CH₄ exchanges. These findings suggest that delineating the peatland heterogeneity in as great detail as possible would be a key to better constrain the estimates of regional CH₄ budget and the climate effect of C exchanges.

4.3. Implication for Mapping Peatland Heterogeneity and Upscaling

Our survey showed that most of the current large-scale land cover products either totally lack or have inappropriate and inaccurate wetland and/or peatland classes. Most of the global products barely detected any peatlands within the study area, and only the national CLC2018FI.20m product had multiple peatland classes, but also it failed to distinguish between noninundated drier and inundated wetter peatlands. Our results showed that upscaling with large-scale land cover products leads to significantly biased estimates of the landscape-scale CO₂, CH₄, and total C budgets of the Kaamanen catchment as compared to the results benefiting from our detailed LCT map (Figure 7). For the CH₄ emission, GLC2000 overestimated and CLC2018FI.20m as well as FROM-GLC10 underestimated substantially, while the other products resulted in a wrong sign of CH₄ flux, that is, net uptake, due to the poor representation of peatlands/wetlands. In the single case (GLC2000) in which the peatland distribution within the Kaamanen catchment was dominated by wetlands that could be translated to our LCTs associated with high CH₄ emissions, their coverage was strongly overestimated and the spatial agreement with our LCT map was only slight (Table 2). The total RE was likely to be overestimated significantly or could even have an incorrect sign (Figure 7). These results imply that, when upscaling C fluxes within the boreal region, the global, continental, and even national land cover products potentially induce significant biases in the estimates of the regional C budgets and their radiative climate effect, which could hamper the prediction of global C-climate feedbacks and the setting of C-neutral targets.

To generate locally most accurate maps of peatland LCTs, it has been shown that ultra-high spatial resolution (pixel size <1 m) airborne or drone data are required (Korpela et al., 2020; Räsänen & Virtanen, 2019). Nevertheless, the use of such data is presently impossible for large regions, but maps based on high-resolution satellite data (pixel size <30 m) are, at least in several cases, sufficient to predict the proportional area of different LCTs (Bartsch et al., 2016; Mahdianpari et al., 2020; Treat et al., 2018). In practice, however, even the national-scale land cover product (CLC2018FI.20m), while showing possible guidelines for larger scale maps and the best performance of the products surveyed in this study, had insufficient accuracy in peatland-type detection.

Both at small and large scales, accurate peatland LCT detection requires multiple remote sensing data sources that bring complementary information, including, for example, optical data depicting spectral properties of land cover, lidar data providing information about topography and vegetation structure, and synthetic aperture radar (SAR) data sensitive to moisture and surface structure (Amani et al., 2017; Bourgeau-Chavez et al., 2017; Hird et al., 2017; Karlson et al., 2019; Mahdianpari et al., 2020; Räsänen & Virtanen, 2019; Räsänen et al., 2021). Freely available high-resolution remote sensing data sets, such as Sentinel-1 SAR, optical Sentinel-2, PlanetScope, and Landsat 8–9, and ArcticDEM topographic data, would enable the generation of circumpolar maps of peatland LCTs. Such maps should be calibrated and validated with spatially extensive local peatland maps, aerial and drone images, and field inventories; conversely, circumpolar maps could be downscaled to locally accurate products with high resolution data sets, such as airborne or drone lidar and multispectral data. Despite these prospects, challenges remain in delineating all relevant peatland LCTs in detail across the entire boreal zone. However, our results indicate that, concerning C budgets, we can make rapid progress and effectively reduce the bias in regional CH₄ flux estimates and related climate effects by emphasizing in land cover classifications a thematic distinction between the noninundated drier peatland and the inundated wetter peatland surface types. To produce circumpolar products, algorithms and sub-pixel classification techniques for peatland type identification should be developed.

5. Conclusions

Based on an extensive set of field and remote sensing data on vegetation, soil, hydrology, and GHG fluxes, we explicitly classified the land cover distribution within a boreal catchment, quantified the C budget and the related

RE both for individual LCTs and the whole catchment, and analyzed the role of peatland heterogeneity in the regional C budget and its radiative climate effect. We find that peatlands dominate the variability of CH₄ flux and the radiative effect that combines CO₂ and CH₄ exchanges among different LCTs. This means that misclassifying peatlands or inadequately representing their true heterogeneity, as was found to be the case in current land cover products, can induce significant biases in the estimates of regional CH₄ budget and radiative effects. However, just distinguishing between the noninundated drier and inundated wetter peatland areas could effectively limit these biases and hence result in a rapid progress in constraining the C-climate nexus.

Data Availability Statement

The data supporting this study are available from Zenodo (<https://zenodo.org/record/6941343>).

Acknowledgments

We are grateful to the two reviewers, Liam Heffernan and Pierre Taillardat, for very constructive comments, which helped us write a better and more interesting manuscript. The authors acknowledge funding from Academy of Finland (CAPTURE Project [#296423, #296887, and #296888]; Atmosphere and Climate Competence Center (ACCC), 337550). D.K. and C.B. were also supported by the Academy of Finland/Russian Foundation for Basic Research project NOCA (decision no. 314630) and the N-PERM project (General Research Grant from the Academy of Finland, decision no. 341348). C.C.T. was supported by ERC #851181 and the Helmholtz Impulse and Networking Fund. J.D. was supported by NASA's Interdisciplinary Research in Earth Science (Grant No. NNX17AK10G). N.C. acknowledges funding from the FORMAS early career grant (contract no. 2019-01151).

References

- Åberg, J., Jansson, M., & Jonsson, A. (2010). Importance of water temperature and thermal stratification dynamics for temporal variation of surface water CO₂ in a boreal lake. *Journal of Geophysical Research*, *115*(G2). <https://doi.org/10.1029/2009JG001085>
- Amani, M., Salehi, B., Mahdavi, S., Granger, J. E., Brisco, B., & Hanson, A. (2017). Wetland classification using multi-source and multi-temporal optical remote sensing data in Newfoundland and Labrador, Canada. *Canadian Journal of Remote Sensing*, *43*(4), 360–373. <https://doi.org/10.1080/07038992.2017.1346468>
- Arino, O., Ramos Perez, J. J., Kalogirou, V., Bontemps, S., Defourny, P., & Van Bogaert, E. (2012). Global land cover map for 2009 (GlobCover 2009). <https://doi.org/10.1594/PANGAEA.787668>
- Aurela, M., Laurila, T., & Tuovinen, J.-P. (2001). Seasonal CO₂ balances of a subarctic mire. *Journal of Geophysical Research*, *106*(D2), 1623–1637. <https://doi.org/10.1029/2000jd900481>
- Aurela, M., Laurila, T., & Tuovinen, J.-P. (2002). Annual CO₂ balance of a subarctic fen in northern Europe: Importance of the wintertime efflux. *Journal of Geophysical Research: Atmospheres*, *107*(D21), ACH17-1–ACH17-12. <https://doi.org/10.1029/2002jd002055>
- Aurela, M., Lohila, A., Tuovinen, J.-P., Hatakka, J., Penttilä, T., & Laurila, T. (2015). Carbon dioxide and energy flux measurements in four northern-boreal ecosystems at Pallas. *Boreal Environment Research*, *20*(4), 455–473.
- Aurela, M., Tuovinen, J. P., & Laurila, T. (2001). Net CO₂ exchange of a subarctic mountain birch ecosystem. *Theoretical and Applied Climatology*, *70*(1), 135–148. <https://doi.org/10.1007/s007040170011>
- Bartholomé, E., & Belward, A. S. (2005). GLC2000: A new approach to global land cover mapping from Earth observation data. *International Journal of Remote Sensing*, *26*(9), 1959–1977. <https://doi.org/10.1080/01431160412331291297>
- Bartsch, A., Hofler, A., Kroisleitner, C., & Trofäier, A. M. (2016). Land cover mapping in northern high latitude permafrost regions with satellite data: Achievements and remaining challenges. *Remote Sensing*, *8*(12), 979. <https://doi.org/10.3390/rs8120979>
- Blaschke, T., Hay, G. J., Kelly, M., Lang, S., Hofmann, P., Addink, E., et al. (2014). Geographic object-based image analysis—Towards a new paradigm. *ISPRS Journal of Photogrammetry and Remote Sensing*, *87*, 180–191. <https://doi.org/10.1016/j.isprsjprs.2013.09.014>
- Boucher, O., Friedlingstein, P., Collins, B., & Shine, K. P. (2009). The indirect global warming potential and global temperature change potential due to methane oxidation. *Environmental Research Letters*, *4*(4), 044007. <https://doi.org/10.1088/1748-9326/4/4/044007>
- Bourgeau-Chavez, L. L., Endres, S., Powell, R., Battaglia, M. J., Benscoter, B., Turetsky, M., et al. (2017). Mapping boreal peatland ecosystem types from multitemporal radar and optical satellite imagery. *Canadian Journal of Forest Research*, *47*(4), 545–559. <https://doi.org/10.1139/cjfr-2016-0192>
- Bradshaw, C. J. A., & Warkentin, I. G. (2015). Global estimates of boreal forest carbon stocks and flux. *Global and Planetary Change*, *128*, 24–30. <https://doi.org/10.1016/j.gloplacha.2015.02.004>
- Breiman, L. (2001). Random forests. *Machine Learning*, *45*(1), 5–32. <https://doi.org/10.1023/a:1010933404324>
- Campeau, A., Lapierre, J. F., Vachon, D., & del Giorgio, P. A. (2014). Regional contribution of CO₂ and CH₄ fluxes from the fluvial network in a lowland boreal landscape of Quebec. *Global Biogeochemical Cycles*, *28*(1), 57–69. <https://doi.org/10.1002/2013gb004685>
- Chapin, F. S., III, Matson, P. A., & Vitousek, P. (2011). *Principles of terrestrial ecosystem ecology*. Springer Science & Business Media.
- Chasmer, L., Cobbaert, D., Mahoney, C., Millard, K., Peters, D., Devito, K., et al. (2020). Remote sensing of boreal wetlands 1: Data use for policy and management. *Remote Sensing*, *12*(8), 1320. <https://doi.org/10.3390/rs12081320>
- Chen, G., Weng, Q., Hay, G. J., & He, Y. (2018). Geographic object-based image analysis (GEOBIA): Emerging trends and future opportunities. *GIScience and Remote Sensing*, *55*(2), 159–182. <https://doi.org/10.1080/15481603.2018.1426092>
- Chi, J., Nilsson, M. B., Laudon, H., Lindroth, A., Wallerman, J., Fransson, J. E. S., et al. (2020). The net landscape carbon balance—Integrating terrestrial and aquatic carbon fluxes in a managed boreal forest landscape in Sweden. *Global Change Biology*, *26*(4), 2353–2367. <https://doi.org/10.1111/gcb.14983>
- Chi, J., Zhao, P., Klosterhalfen, A., Jocher, G., Kljun, N., Nilsson, M. B., & Peichl, M. (2021). Forest floor fluxes drive differences in the carbon balance of contrasting boreal forest stands. *Agricultural and Forest Meteorology*, *306*, 108454. <https://doi.org/10.1016/j.agrformet.2021.108454>
- Christensen, T. R., Johansson, T., Olsrud, M., Strom, L., Lindroth, A., Mastepanov, M., et al. (2007). A catchment-scale carbon and greenhouse gas budget of a subarctic landscape. *Philosophical Transactions of the Royal Society A: Mathematical, Physical & Engineering Sciences*, *365*(1856), 1643–1656. <https://doi.org/10.1098/rsta.2007.2035>
- Clemmensen, K. E., Bahr, A., Ovaskainen, O., Dahlberg, A., Ekblad, A., Wallander, H., et al. (2013). Roots and associated fungi drive long-term carbon sequestration in boreal forest. *Science*, *339*(6127), 1615–1618. <https://doi.org/10.1126/science.1231923>
- Comyn-Platt, E., Hayman, G., Huntingford, C., Chadburn, S. E., Burke, E. J., Harper, A. B., et al. (2018). Carbon budgets for 1.5 and 2°C targets lowered by natural wetland and permafrost feedbacks. *Nature Geoscience*, *11*(8), 568–573. <https://doi.org/10.1038/s41561-018-0174-9>
- Delwiche, K. B., Knox, S. H., Malhotra, A., Fluet-Chouinard, E., McNicol, G., Feron, S., et al. (2021). FLUXNET-CH4: A global, multi-ecosystem dataset and analysis of methane seasonality from freshwater wetlands. *Earth System Science Data*, *13*(7), 3607–3689. <https://doi.org/10.5194/essd-13-3607-2021>
- Dinsmore, K. J., Billett, M. F., Skiba, U. M., Rees, R. M., Drewer, J., & Helfter, C. (2010). Role of the aquatic pathway in the carbon and greenhouse gas budgets of a peatland catchment. *Global Change Biology*, *16*(10), 2750–2762. <https://doi.org/10.1111/j.1365-2486.2009.02119.x>

- Etminan, M., Myhre, G., Highwood, E. J., & Shine, K. P. (2016). Radiative forcing of carbon dioxide, methane, and nitrous oxide: A significant revision of the methane radiative forcing. *Geophysical Research Letters*, *43*(24), 12614–12623. <https://doi.org/10.1002/2016GL071930>
- Frey, K. E., & Smith, L. C. (2007). How well do we know northern land cover? Comparison of four global vegetation and wetland products with a new ground-truth database for west Siberia. *Global Biogeochemical Cycles*, *21*(1). <https://doi.org/10.1029/2006GB002706>
- Friedlingstein, P., O'Sullivan, M., Jones, M. W., Andrew, R. M., Hauck, J., Olsen, A., et al. (2020). Global carbon budget 2020. *Earth System Science Data*, *12*(4), 3269–3340. <https://doi.org/10.5194/essd-12-3269-2020>
- Fronzek, S., Carter, T. R., Raisanen, J., Ruokolainen, L., & Luoto, M. (2010). Applying probabilistic projections of climate change with impact models: A case study for sub-arctic peatlands in Fennoscandia. *Climatic Change*, *99*(3–4), 515–534. <https://doi.org/10.1007/s10584-009-9679-y>
- Gauthier, S., Bernier, P., Kuuluvainen, T., Shvidenko, A. Z., & Schepaschenko, D. G. (2015). Boreal forest health and global change. *Science*, *349*(6250), 819–822. <https://doi.org/10.1126/science.aaa9092>
- Gong, P., Liu, H., Zhang, M., Li, C., Wang, J., Huang, H., et al. (2019). Stable classification with limited sample: Transferring a 30-m resolution sample set collected in 2015 to mapping 10-m resolution global land cover in 2017. *Science Bulletin*, *64*(6), 370–373. <https://doi.org/10.1016/j.scib.2019.03.002>
- Gorham, E. (1991). Northern peatlands: Role in the carbon cycle and probable responses to climatic warming. *Ecological Applications*, *1*(2), 182–195. <https://doi.org/10.2307/1941811>
- Guo, M. Y., Zhuang, Q. L., Tan, Z. L., Shurpali, N., Juutinen, S., Kortelainen, P., & Martikainen, P. J. (2020). Rising methane emissions from boreal lakes due to increasing ice-free days. *Environmental Research Letters*, *15*(6), 064008. <https://doi.org/10.1088/1748-9326/ab8254>
- Halabisky, M., Babcock, C., & Moskal, L. M. (2018). Harnessing the temporal dimension to improve object-based image analysis classification of wetlands. *Remote Sensing*, *10*(9), 1467. <https://doi.org/10.3390/rs10091467>
- Heiskanen, L., Tuovinen, J.-P., Räsänen, A., Virtanen, T., Juutinen, S., Lohila, A., et al. (2021). Carbon dioxide and methane exchange of a patterned subarctic fen during two contrasting growing seasons. *Biogeosciences*, *18*(3), 873–896. <https://doi.org/10.5194/bg-18-873-2021>
- Heiskanen, L., Tuovinen, J.-P., Räsänen, A., Virtanen, T., Juutinen, S., Vekuri, H., et al. (2022). Meteorological responses of carbon dioxide and methane fluxes in the terrestrial and aquatic ecosystems of a subarctic landscape. *Biogeosciences Discussions*, *2022*, 1–45. <https://doi.org/10.5194/bg-2022-69>
- Helbig, M., Waddington, J. M., Alekseychik, P., Amiro, B. D., Aurela, M., Barr, A. G., et al. (2020). Increasing contribution of peatlands to boreal evapotranspiration in a warming climate. *Nature Climate Change*, *10*(6), 555–560. <https://doi.org/10.1038/s41558-020-0763-7>
- Hird, J. N., DeLancey, E. R., McDermid, G. J., & Kariyeva, J. (2017). Google Earth Engine, open-access satellite data, and machine learning in support of large-area probabilistic wetland mapping. *Remote Sensing*, *9*(12), 1315. <https://doi.org/10.3390/rs9121315>
- Hopple, A. M., Wilson, R. M., Kolton, M., Zalman, C. A., Chanton, J. P., Kostka, J., et al. (2020). Massive peatland carbon banks vulnerable to rising temperatures. *Nature Communications*, *11*(1), 2373. <https://doi.org/10.1038/s41467-020-16311-8>
- Hugelius, G., Loisel, J., Chadburn, S., Jackson, R. B., Jones, M., MacDonald, G., et al. (2020). Large stocks of peatland carbon and nitrogen are vulnerable to permafrost thaw. *Proceedings of the National Academy of Sciences of the United States of America*, *117*(34), 20438–20446. <https://doi.org/10.1073/pnas.1916387117>
- Huotari, J., Ojala, A., Peltomaa, E., Nordbo, A., Launiainen, S., Pumpanen, J., et al. (2011). Long-term direct CO₂ flux measurements over a boreal lake: Five years of eddy covariance data. *Geophysical Research Letters*, *38*(18). <https://doi.org/10.1029/2011GL048753>
- Johansson, T., Malmer, N., Crill, P. M., Friborg, T., Akerman, J. H., Mastepanov, M., & Christensen, T. R. (2006). Decadal vegetation changes in a northern peatland, greenhouse gas fluxes and net radiative forcing. *Global Change Biology*, *12*(12), 2352–2369. <https://doi.org/10.1111/j.1365-2486.2006.01267.x>
- Joos, F., Roth, R., Fuglestedt, J. S., Peters, G. P., Enting, I. G., von Bloh, W., et al. (2013). Carbon dioxide and climate impulse response functions for the computation of greenhouse gas metrics: A multi-model analysis. *Atmospheric Chemistry and Physics*, *13*(5), 2793–2825. <https://doi.org/10.5194/acp-13-2793-2013>
- Juutinen, S., Rantakari, M., Kortelainen, P., Huttunen, J. T., Larmola, T., Alm, J., et al. (2009). Methane dynamics in different boreal lake types. *Biogeosciences*, *6*(2), 209–223. <https://doi.org/10.5194/bg-6-209-2009>
- Juutinen, S., Valiranta, M., Kuutti, V., Laine, A. M., Virtanen, T., Seppä, H., et al. (2013). Short-term and long-term carbon dynamics in a northern peatland-stream-lake continuum: A catchment approach. *Journal of Geophysical Research-Biogeosciences*, *118*(1), 171–183. <https://doi.org/10.1002/jgrg.20028>
- Karlson, M., Gålfalk, M., Crill, P., Bousquet, P., Saunio, M., & Bastviken, D. (2019). Delineating northern peatlands using Sentinel-1 time series and terrain indices from local and regional digital elevation models. *Remote Sensing of Environment*, *231*, 111252. <https://doi.org/10.1016/j.rse.2019.111252>
- Kicklighter, D. W., Melillo, J. M., Monier, E., Sokolov, A. P., & Zhuang, Q. L. (2019). Future nitrogen availability and its effect on carbon sequestration in Northern Eurasia. *Nature Communications*, *10*(1), 3024. <https://doi.org/10.1038/s41467-019-10944-0>
- Kljun, N., Black, T. A., Griffiths, T. J., Barr, A. G., Gaumont-Guay, D., Morgenstern, K., et al. (2006). Response of net ecosystem productivity of three boreal forest stands to drought. *Ecosystems*, *9*(7), 1128–1144. <https://doi.org/10.1007/s10021-005-0082-x>
- Kolari, P., Pumpanen, J., Rannik, Ü., Ilvesniemi, H., Hari, P., & Berninger, F. (2004). Carbon balance of different aged Scots pine forests in Southern Finland. *Global Change Biology*, *10*(7), 1106–1119. <https://doi.org/10.1111/j.1529-8817.2003.00797.x>
- Korpela, I., Haapanen, R., Korrensalo, A., Tuittila, E. S., & Vesala, T. (2020). Fine-resolution mapping of microforms of a boreal bog using aerial images and waveform-recording LiDAR. *Mires & Peat*, *26*. <https://doi.org/10.19189/MaP.2018.OMB.388>
- Köster, K., Berninger, F., Linden, A., Köster, E., & Pumpanen, J. (2014). Recovery in fungal biomass is related to decrease in soil organic matter turnover time in a boreal fire chronosequence. *Geoderma*, *235*, 74–82. <https://doi.org/10.1016/j.geoderma.2014.07.001>
- Kou, D., Yang, G., Li, F., Feng, X., Zhang, D., Mao, C., et al. (2020). Progressive nitrogen limitation across the Tibetan alpine permafrost region. *Nature Communications*, *11*(1), 3331. <https://doi.org/10.1038/s41467-020-17169-6>
- Krankina, O. N., Pflugmacher, D., Friedl, M., Cohen, W. B., Nelson, P., & Baccini, A. (2008). Meeting the challenge of mapping peatlands with remotely sensed data. *Biogeosciences*, *5*(6), 1809–1820. <https://doi.org/10.5194/bg-5-1809-2008>
- Kuhn, M. A., Varner, R. K., Bastviken, D., Crill, P., MacIntyre, S., Turetsky, M., et al. (2021). BAWLD-CH4: A comprehensive dataset of methane fluxes from boreal and arctic ecosystems. *Earth System Science Data*, *13*(11), 5151–5189. <https://doi.org/10.5194/essd-13-5151-2021>
- Lawrence, D., Fisher, R., Koven, C., Oleson, K., Swenson, S., Vertenstein, M., et al. (2018). *CLM5.0 technical description*. National Center for Atmospheric Research.
- Lehner, B., & Döll, P. (2004). Development and validation of a global database of lakes, reservoirs and wetlands. *Journal of Hydrology*, *296*(1), 1–22. <https://doi.org/10.1016/j.jhydrol.2004.03.028>
- Li, C. S., Aber, J., Stange, F., Butterbach-Bahl, K., & Papen, H. (2000). A process-oriented model of N₂O and NO emissions from forest soils: 1. Model development. *Journal of Geophysical Research*, *105*(D4), 4369–4384. <https://doi.org/10.1029/1999jd900949>

- Li, T. T., Raivonen, M., Alekseychik, P., Aurela, M., Lohila, A., Zheng, X. H., et al. (2016). Importance of vegetation classes in modeling CH₄ emissions from boreal and subarctic wetlands in Finland. *Science of the Total Environment*, 572, 1111–1122. <https://doi.org/10.1016/j.scitotenv.2016.08.020>
- Lindroth, A., Holst, J., Linderson, M.-L., Aurela, M., Biermann, T., Heliasz, M., et al. (2020). Effects of drought and meteorological forcing on carbon and water fluxes in Nordic forests during the dry summer of 2018. *Philosophical Transactions of the Royal Society B: Biological Sciences*, 375(1810), 20190516. <https://doi.org/10.1098/rstb.2019.0516>
- Lohila, A., Minkinen, K., Laine, J., Savolainen, I., Tuovinen, J.-P., Korhonen, L., et al. (2010). Forestation of boreal peatlands: Impacts of changing albedo and greenhouse gas fluxes on radiative forcing. *Journal of Geophysical Research*, 115(G4), G04011. <https://doi.org/10.1029/2010JG001327>
- Lohila, A., Tuovinen, J.-P., Hatakka, J., Aurela, M., Vuorenmaa, J., Haakana, M., & Laurila, T. (2015). Carbon dioxide and energy fluxes over a northern boreal lake. *Boreal Environment Research*, 20(4), 474–488.
- Loisel, J., Gallego-Sala, A. V., Amesbury, M. J., Magnan, G., Anshari, G., Beilman, D. W., et al. (2021). Expert assessment of future vulnerability of the global peatland carbon sink. *Nature Climate Change*, 11(1), 70–77. <https://doi.org/10.1038/s41558-020-00944-0>
- Loveland, T. R., Reed, B. C., Brown, J. F., Ohlen, D. O., Zhu, Z., Yang, L., & Merchant, J. W. (2000). Development of a global land cover characteristics database and IGBP DISCover from 1 km AVHRR data. *International Journal of Remote Sensing*, 21(6–7), 1303–1330. <https://doi.org/10.1080/014311600210191>
- Mahdianpari, M., Salehi, B., Mohammadmanesh, F., Brisco, B., Homayouni, S., Gill, E., et al. (2020). Big data for a big country: The first generation of Canadian wetland inventory map at a spatial resolution of 10-m using Sentinel-1 and Sentinel-2 data on the Google Earth engine cloud computing platform. *Canadian Journal of Remote Sensing*, 46(1), 15–33. <https://doi.org/10.1080/07038992.2019.1711366>
- Mathijssen, P. J. H., Kahkola, N., Tuovinen, J.-P., Lohila, A., Minkinen, K., Laurila, T., & Valiranta, M. (2017). Lateral expansion and carbon exchange of a boreal peatland in Finland resulting in 7000 years of positive radiative forcing. *Journal of Geophysical Research-Biogeosciences*, 122(3), 562–577. <https://doi.org/10.1002/2016jg003749>
- Matthews, E., Johnson, M. S., Genovesi, V., Du, J., & Bastviken, D. (2020). Methane emission from high latitude lakes: Methane-centric lake classification and satellite-driven annual cycle of emissions. *Scientific Reports*, 10(1), 12465. <https://doi.org/10.1038/s41598-020-68246-1>
- Meinshausen, M., Smith, S. J., Calvin, K., Daniel, J. S., Kainuma, M. L. T., Lamarque, J. F., et al. (2011). The RCP greenhouse gas concentrations and their extensions from 1765 to 2300. *Climatic Change*, 109(1), 213–241. <https://doi.org/10.1007/s10584-011-0156-z>
- Myhre, G., Shindell, D., Bréon, F. M., Collins, W., Fuglestedt, J., Huang, J., et al. (2013). Anthropogenic and natural radiative forcing. In T. F. Stocker, D. Qin, G.-K. Plattner, M. Tignor, S. K. Allen, J. Boschung, et al. (Eds.), *Climate change 2013: The physical science basis. Contribution of working group I to the fifth assessment report of the intergovernmental panel on climate change*. Cambridge University Press.
- Natali, S. M., Watts, J. D., Rogers, B. M., Potter, S., Ludwig, S. M., Selbmann, A. K., et al. (2019). Large loss of CO₂ in winter observed across the northern permafrost region. *Nature Climate Change*, 9(11), 852–857. <https://doi.org/10.1038/s41558-019-0592-8>
- Neubauer, S. C. (2021). Global warming potential is not an ecosystem property. *Ecosystems*, 24(8), 2079–2089. <https://doi.org/10.1007/s10021-021-00631-x>
- Olefeldt, D., Hovemyr, M., Kuhn, M. A., Bastviken, D., Bohn, T. J., Connolly, J., et al. (2021). The Boreal–Arctic Wetland and Lake Dataset (BAWLD). *Earth System Science Data*, 13(11), 5127–5149. <https://doi.org/10.5194/essd-13-5127-2021>
- Olson, D. M., Dinerstein, E., Wikramanayake, E. D., Burgess, N. D., Powell, G. V. N., Underwood, E. C., et al. (2001). Terrestrial ecoregions of the world: A new map of Life on Earth: A new global map of terrestrial ecoregions provides an innovative tool for conserving biodiversity. *BioScience*, 51(11), 933–938. [https://doi.org/10.1641/0006-3568\(2001\)051\[0933:TEOTWA\]2.0.CO;2](https://doi.org/10.1641/0006-3568(2001)051[0933:TEOTWA]2.0.CO;2)
- O'Shea, S. J., Allen, G., Gallagher, M. W., Bower, K., Illingworth, S. M., Muller, J. B. A., et al. (2014). Methane and carbon dioxide fluxes and their regional scalability for the European Arctic wetlands during the MAMM project in summer 2012. *Atmospheric Chemistry and Physics*, 14(23), 13159–13174. <https://doi.org/10.5194/acp-14-13159-2014>
- Piilo, S. R., Korhola, A., Heiskanen, L., Tuovinen, J.-P., Aurela, M., Juutinen, S., et al. (2020). Spatially varying peatland initiation, Holocene development, carbon accumulation patterns and radiative forcing within a subarctic fen. *Quaternary Science Reviews*, 248, 106596. <https://doi.org/10.1016/j.quascirev.2020.106596>
- Pirinen, P., Simola, H., Aalto, J., Kaukoranta, J.-P., Karlsson, P. S., & Ruuhela, R. (2012). *Climatological statistics of Finland 1981–2010, reports 2012:1*. Finnish Meteorological Institute.
- Räsänen, A., Juutinen, S., Tuittila, E. S., Aurela, M., & Virtanen, T. (2019). Comparing ultra-high spatial resolution remote-sensing methods in mapping peatland vegetation. *Journal of Vegetation Science*, 30(5), 1016–1026. <https://doi.org/10.1111/jvs.12769>
- Räsänen, A., Manninen, T., Korkiakoski, M., Lohila, A., & Virtanen, T. (2021). Predicting catchment-scale methane fluxes with multi-source remote sensing. *Landscape Ecology*, 36(4), 1177–1195. <https://doi.org/10.1007/s10980-021-01194-x>
- Räsänen, A., & Virtanen, T. (2019). Data and resolution requirements in mapping vegetation in spatially heterogeneous landscapes. *Remote Sensing of Environment*, 230, 111207. <https://doi.org/10.1016/j.rse.2019.05.026>
- Sturtevant, C. S., & Oechel, W. C. (2013). Spatial variation in landscape-level CO₂ and CH₄ fluxes from arctic coastal tundra: Influence from vegetation, wetness, and the thaw lake cycle. *Global Change Biology*, 19(9), 2853–2866. <https://doi.org/10.1111/gcb.12247>
- Sulla-Menashe, D., Gray, J. M., Abercrombie, S. P., & Friedl, M. A. (2019). Hierarchical mapping of annual global land cover 2001 to present: The MODIS Collection 6 Land Cover product. *Remote Sensing of Environment*, 222, 183–194. <https://doi.org/10.1016/j.rse.2018.12.013>
- Tageson, T., Schurgers, G., Horion, S., Ciais, P., Tian, F., Brandt, M., et al. (2020). Predict divergence in the contributions of tropical and boreal forests to the terrestrial carbon sink. *Nature Ecology & Evolution*, 4(2), 202–209. <https://doi.org/10.1038/s41559-019-1090-0>
- Taillardat, P., Thompson, B. S., Garneau, M., Trottier, K., & Friess, D. A. (2020). Climate change mitigation potential of wetlands and the cost-effectiveness of their restoration. *Interface Focus*, 10(5), 20190129. <https://doi.org/10.1098/rsfs.2019.0129>
- Tan, Z., Zhuang, Q., & Anthony, K. W. (2015). Modeling methane emissions from arctic lakes: Model development and site-level study. *Journal of Advances in Modeling Earth Systems*, 7(2), 459–483. <https://doi.org/10.1002/2014ms000344>
- Tan, Z., Zhuang, Q., Shurpali, N. J., Marushchak, M. E., Biasi, C., Eugster, W., & Anthony, K. W. (2017). Modeling CO₂ emissions from Arctic lakes: Model development and site-level study. *Journal of Advances in Modeling Earth Systems*, 9(5), 2190–2213. <https://doi.org/10.1002/2017ms001028>
- Tang, J., Miller, P. A., Persson, A., Olefeldt, D., Pileso, P., Heliasz, M., et al. (2015). Carbon budget estimation of a subarctic catchment using a dynamic ecosystem model at high spatial resolution. *Biogeosciences*, 12(9), 2791–2808. <https://doi.org/10.5194/bg-12-2791-2015>
- Tanneberger, F., Tegetmeyer, C., Busse, S., Barthelmes, A., Shumka, S., Marine, A. M., et al. (2017). The peatland map of Europe. *Mires & Peat*, 19. <https://doi.org/10.19189/Map.2016.OMB.264>
- Thompson, D. K., Simpson, B. N., & Beaudoin, A. (2016). Using forest structure to predict the distribution of treed boreal peatlands in Canada. *Forest Ecology and Management*, 372, 19–27. <https://doi.org/10.1016/j.foreco.2016.03.056>

- Treat, C. C., Bloom, A. A., & Marushchak, M. E. (2018). Nongrowing season methane emissions - A significant component of annual emissions across northern ecosystems. *Global Change Biology*, 24(8), 3331–3343. <https://doi.org/10.1111/gcb.14137>
- Treat, C. C., Marushchak, M. E., Voigt, C., Zhang, Y., Tan, Z., Zhuang, Q., et al. (2018). Tundra landscape heterogeneity, not interannual variability, controls the decadal regional carbon balance in the western Russian Arctic. *Global Change Biology*, 24(11), 5188–5204. <https://doi.org/10.1111/gcb.14421>
- Verpoorter, C., Kutser, T., Seekell, D. A., & Tranvik, L. J. (2014). A global inventory of lakes based on high-resolution satellite imagery. *Geophysical Research Letters*, 41(18), 6396–6402. <https://doi.org/10.1002/2014GL060641>
- Virkkala, A.-M., Aalto, J., Rogers, B. M., Tagesson, T., Treat, C. C., Natali, S. M., et al. (2021). Statistical upscaling of ecosystem CO₂ fluxes across the terrestrial tundra and boreal domain: Regional patterns and uncertainties. *Global Change Biology*, 27(17), 4040–4059. <https://doi.org/10.1111/gcb.15659>
- Weller, G., Chapin, F. S., Everett, K. R., Hobbie, J. E., Kane, D., Oechel, W. C., et al. (1995). The arctic flux study: A regional view of trace gas release. *Journal of Biogeography*, 22(2–3), 365–374. <https://doi.org/10.2307/2845932>
- Xu, J. R., Morris, P. J., Liu, J. G., & Holden, J. (2018). PEATMAP: Refining estimates of global peatland distribution based on a meta-analysis. *Catena*, 160, 134–140. <https://doi.org/10.1016/j.catena.2017.09.010>
- Zhang, Y., Chen, W. J., & Cihlar, J. (2003). A process-based model for quantifying the impact of climate change on permafrost thermal regimes. *Journal of Geophysical Research*, 108(D22), 4695. <https://doi.org/10.1029/2002jd003354>
- Zhang, Y., Sachs, T., Li, C., & Boike, J. (2012). Upscaling methane fluxes from closed chambers to eddy covariance based on a permafrost biogeochemistry integrated model. *Global Change Biology*, 18(4), 1428–1440. <https://doi.org/10.1111/j.1365-2486.2011.02587.x>

References From the Supporting Information

- Böhner, J., & Selige, T. (2006). Spatial prediction of soil attributes using terrain analysis and climate regionalisation. *Gottinger Geographische Abhandlungen*, 115, 13–28.
- Gitelson, A. A., Kaufman, Y. J., Stark, R., & Rundquist, D. (2002). Novel algorithms for remote estimation of vegetation fraction. *Remote Sensing of Environment*, 80(1), 76–87. [https://doi.org/10.1016/s0034-4257\(01\)00289-9](https://doi.org/10.1016/s0034-4257(01)00289-9)
- Guisan, A., Weiss, S. B., & Weiss, A. D. (1999). GLM versus CCA spatial modeling of plant species distribution. *Plant Ecology*, 143(1), 107–122. <https://doi.org/10.1023/a:1009841519580>
- Haralick, R. M., Shanmugam, K., & Dinstein, I. H. (1973). Textural features for image classification. *IEEE Transactions on systems, man, and cybernetics*, SMC-, 3(6), 610–621. <https://doi.org/10.1109/tsmc.1973.4309314>
- McFeeters, S. K. (1996). The use of the Normalized Difference Water Index (NDWI) in the delineation of open water features. *International Journal of Remote Sensing*, 17(7), 1425–1432. <https://doi.org/10.1080/01431169608948714>
- Repola, J. (2008). Biomass equations for birch in Finland. *Silva Fennica*, 42(4), 605–624. <https://doi.org/10.14214/sf.236>
- Repola, J. (2009). Biomass equations for Scots pine and Norway spruce in Finland. *Silva Fennica*, 43(4), 625–647. <https://doi.org/10.14214/sf.184>
- Rouse, J. W., Jr., Haas, R. H., Schell, J. A., & Deering, D. W. (1973). Monitoring vegetation systems in the great plains with ERTS. In S. C. Freden, E. P. Mercanti, & M. A. Becker (Eds.), *Third Earth resources technology satellite-1 symposium*. NASA Special Publication.
- Treat, C. C., Marushchak, M. E., Voigt, C., Zhang, Y., Tan, Z., Zhuang, Q., et al. (2018). Tundra landscape heterogeneity, not interannual variability, controls the decadal regional carbon balance in the Western Russian Arctic. *Global Change Biology*, 24(11), 5188–5204. <https://doi.org/10.1111/gcb.14421>